Master's Thesis of Engineering

Strength of Steel Column Subjected to Thermal Gradient Loading under Fire

화재시 단면내 온도구배 하중을 받는
강재기둥의 강도 해석

August 2023

Graduate School of Engineering
Seoul National University
Architecture and Architectural Engineering

Won So

Strength of Steel Column Subjected to Thermal Gradient Loading under Fire

Advisor: Cheol-Ho Lee

Submitting a master's thesis of
Architecture and Architectural Engineering

August 2023

Graduate School of Engineering
Seoul National University
Architecture and Architectural Engineering

Won So

Confirming the master's thesis written by
Won So

August 2023

Chair	**SUNG-GUL HONG**	**(Seal)**
Vice Chair	**CHEOL-HO LEE**	**(Seal)**
Examiner	**HONG-GUN PARK**	**(Seal)**

Abstract

Strength of Steel Column Subjected to Thermal Gradient Loading under Fire

So, Won

Department of Architecture and Architectural Engineering

College of Engineering

Seoul National University

When steel column is exposed to compartment fire, the thermal gradient across the cross-section occurs for several reasons, such as non-homogeneous fire properties, thermal separation by firewall, or loss of fire protection due to aging. The column with thermal gradient bends toward hotter side due to uneven thermal expansion, called thermal bowing, while the center of stiffness shifts from the geometric centroid to cooler side. These phenomena cause load eccentricity, which have negative effects on the performance of the column. Current design standards do not provide specific methods to account for the impact of thermal gradients.

In this study, heat transfer analysis was conducted for five different heating conditions, which assume realistic fire situation, and the thermal gradient patterns in H-shape steel section were analyzed. It was shown that the thermal

gradient patterns can be classified into three types: high-temperature dominant, linear, and low-temperature dominant types. Based on the heat transfer analysis, a simple equation for predicting the eccentricity with maximum and minimum temperatures is proposed. For each heating condition, structural finite element analysis of columns with various load ratios are performed. As a result, despite lower average and maximum temperatures of thermal gradient, the fire resistance ratings (FRR) may be shorter due to the steep thermal gradient. P-M interaction between the compressive force and the bending moment according to the eccentricity due to the thermal gradient was proposed, and the strength of the column with the thermal gradient was predicted as safe compared to the existing design equation.

Keywords : fire resistance; thermal gradient; thermal bowing; column eccentricity; steel columns;

Student Number : 2021-29074

Contents

List of Tables

List of Figures

Chapter 1. Introduction

1.1 Research Background

Considering that fires primarily occur in buildings, it is important to investigate the behavior of key structural elements, such as columns, during a fire event. However, variables make it difficult to predict structural response, such as fire compartments, combustible contents, ventilation conditions and others. when a fire occurs within a fire compartment, the fire spreads from the ignition point, resulting in non-uniform heating of the entire structure. Consequently, it produces a temperature gradient through the cross-section of structural members, including columns and beams. Steel has higher thermal conductivity compared to concrete, so that temperature heats up rapidly in a fire, which leads to a rapid decrease in material strength and stiffness. As a result, the thermal gradients across the cross-sections of steel columns not only affect their fire resistance performance but also have significant impacts on their structural performance.

In spite of these impacts, current design standards do not consider the effects of thermal deformations. In AISC 360 (2022), it prescribes that columns subjected to uniform heating have much greater heat influx, uniformly heated columns reached their failure temperature earlier than non-uniform heated columns with thermal gradients. In other words, they argue that non-uniform heated columns can be neglected based on analysis by Agarwal. However, the

study (Agarwal et al., 2014) considered only steel with no fire protective material. If considering the case of steel with fire protection, it can't be ensured that thermal gradients can be neglected. On the other hand, Eurocode-3 (EN 1993-1-2, 2005) prescribes that the effects of thermal deformations should be considered but there is No specific guidance about design. Therefore, it is necessary to investigate the thermal gradient patterns occurring over the cross-section of the steel column and analyze their effects on the column.

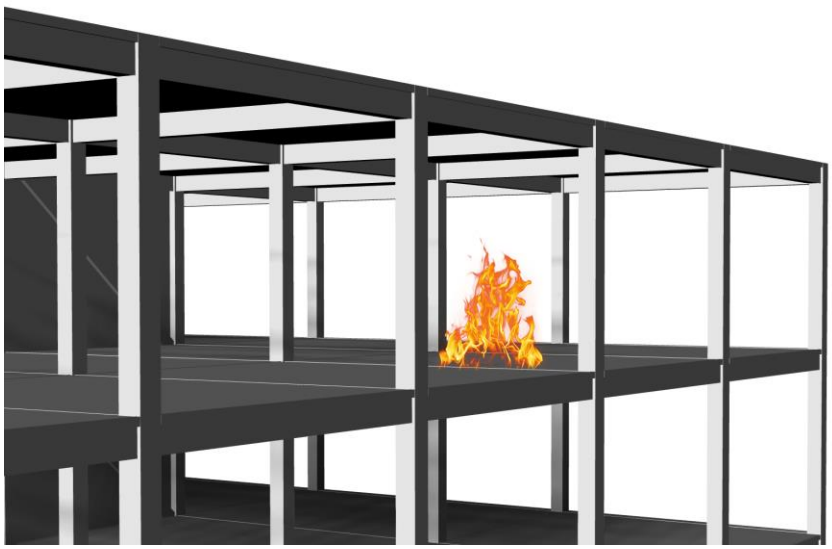

Figure 1.1 Uneven heating in structure

1.1.1 Causes of eccentricity due to thermal gradient

This study focuses on understanding the effects of thermal gradients over the cross-section of a steel column when subjected to non-uniform heating. The thermal gradients over the cross-section induce eccentricity, causing the load

that was originally applied at geometric centroid to become eccentric load, resulting in additional moments in the column. These additional moments have significant impacts on behavior of the column at elevated temperature. Two factors of the columns complicate the buckling behavior. : ① Shift of stiffness center, ② Thermal bowing.

First, eccentricity occurs due to the shift of the stiffness center over the column cross-section. This is attributed to the variation in elastic modulus and yield stress of steel with elevated temperatures. As the temperature of the steel increases during a fire, its stiffness decreases compared to stiffness at room temperature. Therefore, thermal gradients across the cross-section lead to uneven stiffness through the section. As a result, the stiffness center, initially positioned at the geometric centroid without thermal gradients, shifts towards the cooler side (the side with higher stiffness) due to thermal gradients. Figure 1.2 shows the shift of stiffness center (e_c).

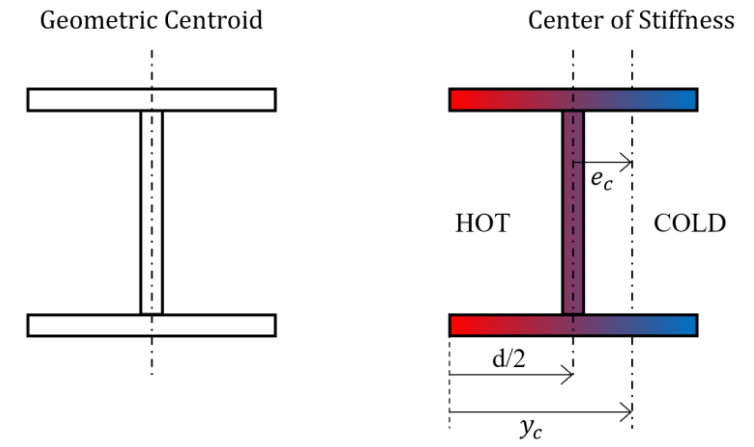

(a) Steel section at room temperature

(b) Steel section after fire

Figure 1.2 Shift of stiffness center

Second, eccentricity occurs due to thermal bowing. When steel is subjected to uneven heating, the hotter side of the column experiences greater expansion than the cooler side. Consequently, the column bends or bows towards the hotter side by e_b. (Figure 1.3)

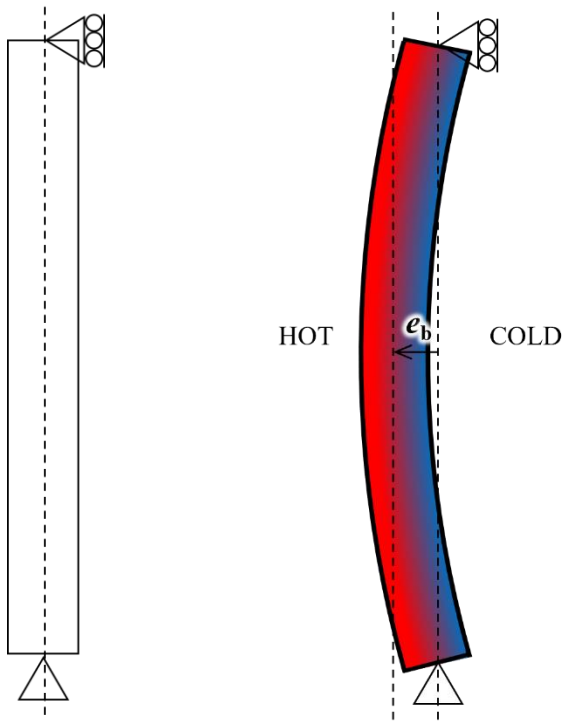

(a) steel at room temperature (b) steel after fire

Figure 1.3 Thermal bowing

1.1.2 Total eccentricity

Two factors inducing eccentricity due to thermal gradients across the cross-

section show distinct trends.

The shift of the stiffness center occurs towards the cooler side, as it moves towards the side with higher stiffness. However, the eccentricity due to thermal bowing occurs towards the hotter side, causing greater expansion. These two eccentricities occur in opposite directions, resulting in an offset effect. The final direction of eccentricity is determined by the more influential factor.

The eccentricity due to thermal bowing (e_b) is proportional to the square of the column length (L). Therefore, the behavior of slenderer columns is primarily governed by thermal bowing, resulting in bending towards the hotter side. Conversely, the eccentricity due to the shift of the stiffness center (e_c) is solely influenced by the thermal gradient, regardless of the column length (L). As a result, the behavior of very short columns is primarily governed by the shift of the stiffness center, leading to eccentricity towards the cooler side.

In addition, the total eccentricity includes the eccentricity due to initial imperfections (e_i). The initial imperfections were considered by 1/1000 of the column length L. Both directions of initial imperfections are considered when calculating the total eccentricity Consequently, the total eccentricity can be calculated as Eq. (1.1). Schematic of total eccentricity is shown in Figure 1.4.

$$e = \max(e_{\mathrm{c}} - e_{\mathrm{b}} + e_{\mathrm{i}},\quad e_{\mathrm{b}} - e_{\mathrm{c}} + e_{\mathrm{i}}) \tag{1.1}$$

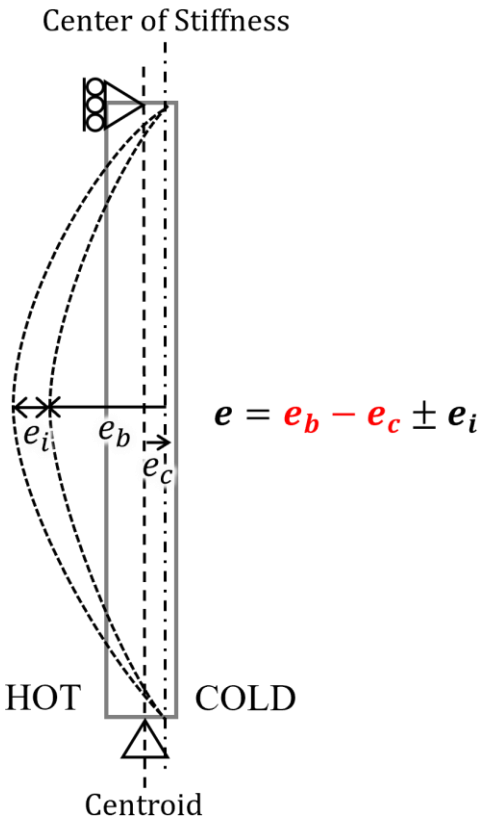

Figure 1.4 Fire-induced eccentricity

1.2 Objectives and Outlines

The final objective of this study is to investigate the impact of eccentricity induced by thermal gradients over the cross-section of the column. First, numerical analysis was performed to simulate the actual fire scenario and conduct heat transfer analysis. Various temperature distributions that can occur over the cross-section were obtained from the heat transfer analysis. Based on these results, four types of simple schematic thermal gradients were assumed, and eccentricities were theoretically calculated based on Mechanics of Materials.

The theoretically calculated eccentricities can be divided into two components: eccentricity due to the shift of the stiffness center and eccentricity due to thermal bowing. The equations for these two eccentricities of H-shaped section are highly complex, making it difficult for hand calculations and considering the eccentricity into design or research. Therefore, a simple equation for calculating the eccentricity was proposed through trend analysis. Furthermore, by comparing the eccentricity calculated by the proposed equation with the actual fire-induced eccentricity using the temperature data obtained from the heat transfer analysis, it proved that the value from the proposed equation accurately predicts the actual eccentricity.

Lastly, the fire resistance and strength for the columns with fire-induced eccentricity were analyzed through load-heating analysis. In other words, the relationship between the fire-induced eccentricity and the strength of the columns at the elevated-temperature was analyzed using the *P-M* interaction.

In this study, H-shaped sections (H-400x400x13x21, H-300x300x10x15, and H-200x200x8x12) are covered, but the eccentricity due to thermal gradients is independent of the section size. Therefore, only H-400x400x13x21 is chosen for analysis. Although the calculations for eccentricity was applied to only H-400x400x13x21, it can be assumed that the same results can be obtained for other section sizes as well. The mechanical properties (the elastic modulus and yield strength) of steel were used as E=210 GPa and f_y=355 MPa, and the thermal properties of the steel at the elevated temperature are taken as specified in the Eurocode-3.

Table 1.1 Scope of the thesis

Section type	H x B	t_1	t_2	E [GPa]	f_y [MPa]
H	400 x 400	13	21	210	355

Chapter 2. Literature Review

2.1 Current design standards

The effects of thermal gradients are explicitly mentioned in Eurocode-3 and AISC 360 as follows. In EN 1993-1-2: 2.4.2 Member analysis, it is stipulated that the effects of thermal deformations resulting from thermal gradients across the cross-section need to be considered. However, there is no specific method provided for considering thermal gradients. In AISC 360-22: APPENDIX 4 Structural design for fire conditions, it is stipulated that if average temperature is same, thermal gradients reduce strength of the column. However, columns subjected to uniform heating have much greater heat influx, uniformly heated columns reached their failure temperature earlier than non-uniform heated columns with thermal gradients. (Figure 2.1) That is, non-uniformly heated columns can be ignored, and it is possible to model the thermal response of steel using the temperature equal to the maximum steel temperature. This conclusion is derived from Agarwal's analysis (Agarwal et al., 2014).

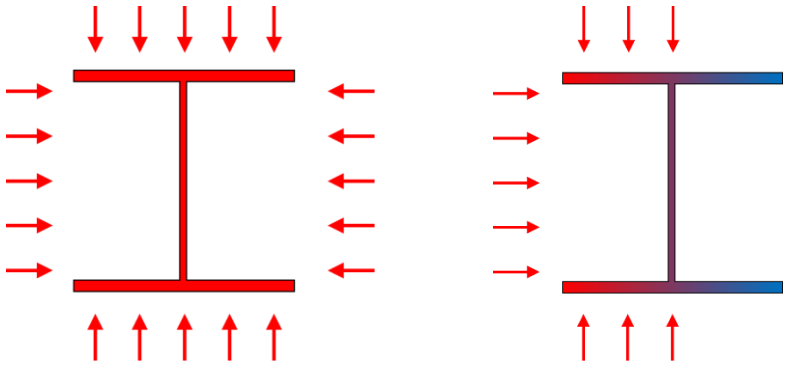

(a) Uniform heating (b) Non-uniform heating

Figure 2.1 Heat influx for (a) uniform and (b) non-uniform heating

However, considering different previous studies that examine various fire scenarios, as discussed below in Section 2.2.1, it cannot be assured that uniformly heated columns reach the failure temperature earlier than the column with thermal gradients. If it is designed using temperature equal to the maximum steel temperature as stipulated in AISC 360-22, it will result in a significantly lower strength compared to designing considering the thermal gradient in fire. This approach makes the design overly conservative. As a result, as specified in the Eurocode-3 (EN 1993-1-2, 2005), the effect of the thermal gradient must be considered.

2.2 Previous studies

2.2.1 Heating configurations

In Agarwal's study (Agarwal et al., 2014), column sections were subjected to three different types of fire loading for heat transfer analysis : 1) heated from all sides, 2) thermal gradient along the web, and 3) thermal gradient along the flange. They did not consider the fire protective material. As a result, uniform heating from all sides leads to a greater heat influx, it is expected that uniformly heated columns reach failure faster than unevenly heated columns.

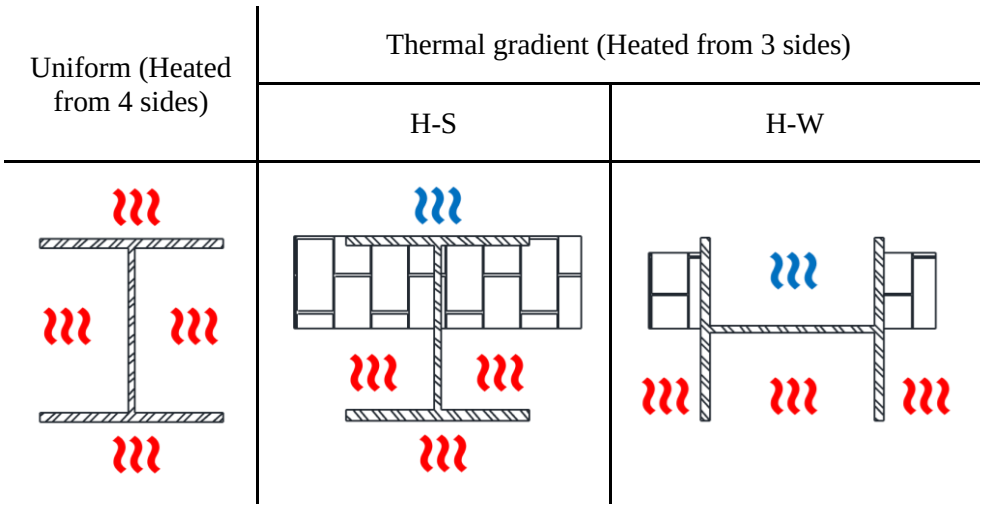

Figure 2.2 Schematics of the heating configurations in Agarwal's analysis

Meanwhile, Dwaikat's analysis (Dwaikat et al., 2012) considered the fire protective material such as insulation. Uniform spray applied fire protection material and 5% loss of fire protection in one flange of the column are compared in terms of fire resistance and strength of column. As the results, 5% loss of insulation can reduce fire resistance of a steel column from 3hr to 90min.

Furthermore, the capacity drops to 50% after 100min of exposure when 5% of insulation is lost. It means that the partial loss of insulation has a significant impact on the bearing capacity and hence fire resistance of structural members. Therefore, the effects of thermal gradient cannot be neglected.

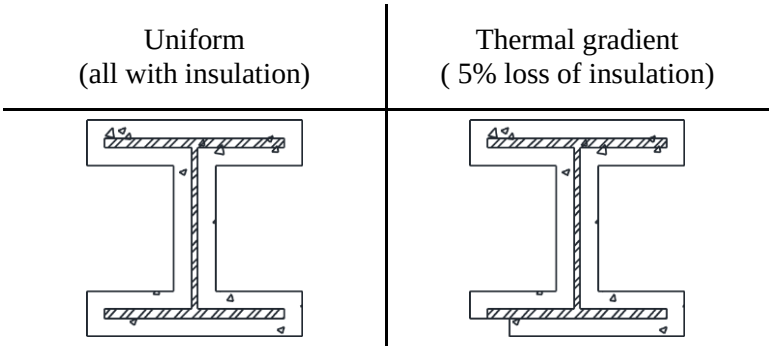

Figure 2.3 Schematics of the heating configurations in Dwaikat's analysis

2.2.2 Longitudinally non-uniform temperature distribution

Becker's analysis (Becker, 2002) focuses on the effects of longitudinally non-uniform temperature distributions on structural fire response up to failure of thermally protected steel structures, composed of beams and columns in simple frame situations.(Figure 2.4) Table 2.1 presents the results for the fire resistance achieved in all assumed cases, including the maximum temperature values at the central main part of the relevant members at the point of failure. It is evident that the longitudinally non-uniform temperature distributions lead to a significant temperature increase at the main central parts prior to failure initiation.

In Becker's paper (Becker, 2002), it can be found that the fire resistance of

columns with longitudinally non-uniform temperature distribution was approximately 16% larger than that of columns with uniform temperature distribution. When subjected to longitudinally uniform temperature distribution, the column can resist for 61-63 min and reach a temperature of 580℃. Meanwhile, the non-uniformly heated columns can resist for 71-73 min and reach temperatures up to 650℃.

A structurally safe design of steel structures is possible by considering only the inherent longitudinal temperature uniformity that has low fire resistances. As a result, our study only considered the longitudinally uniform temperature distribution.

Table 2.1 The results of longitudinally uniform and non-uniform

Description of analysis method and case	Predicted fire resistance (min)	Temperature upon failure at main parts (℃)
FE analysis for case A with longitudinally **uniform** temperature distribution	63	591
FE analysis for case A with longitudinally **non-uniform** temperature distribution	73	656
FE analysis for case C with longitudinally **uniform** temperature distribution	61	577
FE analysis for case C with longitudinally **non-uniform** temperature distribution	71	640
FE analysis for case D with longitudinally **uniform** temperature distribution	79	607
FE analysis for case D with longitudinally **non-uniform** temperature distribution	81	619
FE analysis for case D with longitudinally **uniform** temperature distribution	62	Beam : 584 (Column: 504)
FE analysis for case D with longitudinally **non-uniform** temperature distribution	72	Beam : 650 (Column: 567)

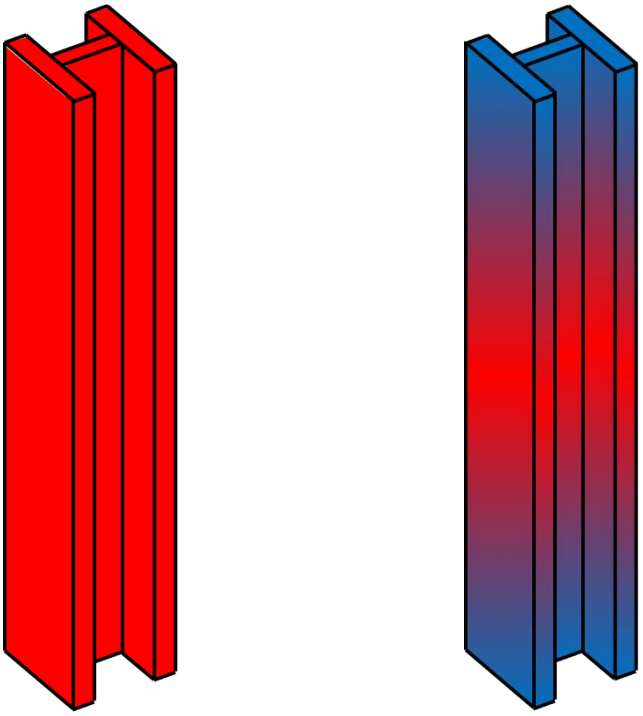

(a) Longitudinally uniform heating

(b) Longitudinally non-uniform heating

Figure 2.4 Analysis of longitudinal thermal gradient

2.2.3 Residual stress

As a steel column with residual stress yields before reaching the nominal yield strength at room temperature, it is essential to consider the residual stress in the column's strength at room temperature. In Yang K-C's study (Yang et al., 2009), a series of experimental studies was conducted to examine the behavior of SN490 steel columns subjected to axial load under fire conditions. The objective of this experimental work was to investigate the effect of residual stress in fire events.

Table 2.2 includes twelve specimens (Specimen Nos. 1–12) designed as stub columns with 3 types of width-to-thickness ratios. As shown in the table, the ratio of the experimental column strengths (P_{exp}) and the yield load (P_{yT}) is all greater than 1. The yield load at temperature T (P_{yT}) is defined as the yield stress with the temperature-dependent material properties multiplied by the area of the cross-section.

As can be seen from Table 2.2, the residual stress is nearly released at high temperatures. At room temperature, the residual stress accounts for more than 20% of the yield stress, but at high temperatures, it is observed that the residual stress is considerably reduced to less than 10%. With the release of residual stress in the fire condition, the effect of residual stress on column strength can be neglected.

Table 2.2 Experimental results of stub column specimens

No.	Dimensions of Specimen	b/t	Test temperature(℃)	P_{exp}/P_{yT}	P_{exp}/P_n	$F_{r,max}/F_y$
1	H-110 x 110 x 8 x 8	7	Room temperature	1.43	1.55	0.33
2			500	1.66	1.13	0.01
3			550	1.49	0.79	0.02
4			600	1.28	0.52	0.02
5	H-130 x 130 x 8 x 8	8	Room temperature	1.30	1.40	0.22
6			500	1.56	1.06	0.01
7			550	1.40	0.74	0.06
8			600	1.22	0.49	0.06
9	H-180 x 180 x 8 x 8	11	Room temperature	1.12	1.20	0.23
10			500	1.21	0.80	0.11
11			550	1.29	0.68	0.08
12			600	1.18	0.48	0.05

2.2.4 *P-M* interaction considering eccentricity

In two previous analysis, P-M interaction curve considering the eccentricity due to thermal gradient is proposed. In Ojeda's analysis (Ojeda et al., 2016), the design equation using strength of column at elevated temperature in Eurocode-3 (EN 1993-1-2, 2005) is proposed as follow Eq. (2.1).

$$\frac{P_{\text{grad}}}{\chi_{\theta_{\text{av}}} \cdot P_{\text{y},\theta_{\text{av}}}} + \kappa \frac{e \cdot P_{\text{grad}}}{M_{\text{p},\theta_{\text{av}}}} \leq 1 \tag{2.1}$$

where : P_{grad} = the load capacity of column subjected to thermal gradient; $\chi_{\theta_{\text{av}}}$ = buckling factor of a centrally loaded column with material properties at average elevated temperature, θ_{av} from Eq. (2.2); e = eccentricity from Eq. (2.5); κ = interaction factor from Eq. (2.8); $M_{\text{p},\theta_{\text{av}}}$ = plastic moment with material properties at the average temperature, θ_{av} .

The buckling factor for a centrally loaded column in Eq. (2.2), $\chi_{\theta_{\text{av}}}$, is a slightly modified version of the equation provided in Eurocode-3 (EN 1993-1-2, 2005).

$$\chi_{\theta_{\text{av}}} = \frac{1}{\phi_{\theta_{\text{av}}} + \sqrt{\phi_{\theta_{\text{av}}}^{\,2} - \overline{\lambda}_{\theta_{\text{av}}}^{\,2}}} \tag{2.2}$$

$$\phi_{\theta_{\text{av}}} = \frac{1}{2}\left(1 + \overline{\lambda}_{\theta_{\text{av}}} \sqrt{\frac{235 N/\text{mm}^2}{f_{\text{y}}}} + \overline{\lambda}_{\theta_{\text{av}}}^{\,2}\right) \tag{2.3}$$

$$\overline{\lambda}_{\theta_{\text{av}}} = \sqrt{\frac{A \cdot f_{\text{y},\theta_{\text{av}}}}{P_{\text{e},\theta_{\text{av}}}}} \tag{2.4}$$

Where: $\phi_{\theta_{\text{av}}}$ = coefficient in the buckling equation; f_{y} = yield stress at room temperature; $\overline{\lambda}_{\theta_{\text{av}}}$ = relative slenderness according to Eq. (2.4) with yield stress and modulus of elasticity at average elevated temperature.

The eccentricity, e in Eq.(2.5), consist of the consists of the sum of the initial imperfection, e_{i}, thermal bowing eccentricity, e_{b}, and the distance between the shifted neutral axis and the load application point, e_{c}. An approximate equation is considered for the eccentricity which is the maximum of eccentricities e_1 and e_2 indicated in Figure 2.5.

$$e = \max(e_1, e_2) \tag{2.5}$$

$$e_1 = e_{\mathrm{c}} \tag{2.6}$$

$$e_2 = e_{\mathrm{b}} - e_{\mathrm{c}} + e_{\mathrm{i}} \tag{2.7}$$

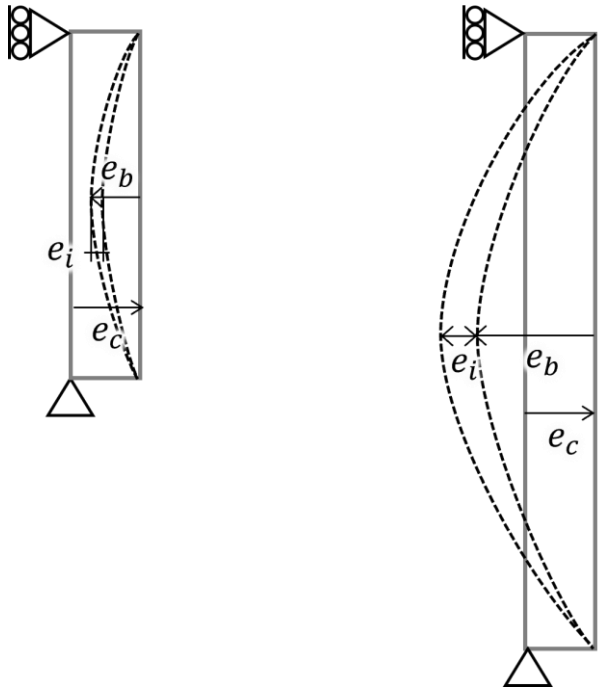

Figure 2.5 Eccentricity from Ojeda et al. (2016)

The interaction factor, κ in Eq. (2.8), is a modified version of the factor provided in Talamona D et al. (1997).

$$\kappa = -7\left(\frac{P_{\text{grad}}}{P_{\text{y},\theta_{\text{av}}}}\right)^2 + 7\left(\frac{P_{\text{grad}}}{P_{\text{y},\theta_{\text{av}}}}\right) - 0.55 \tag{2.8}$$

In Agarwal's analysis, the design equation using strength of column at room temperature in AISC 360 is proposed as follow Eq. (2.9).

$$\frac{P_{\text{grad}}}{P_{\text{cr,eff}}} + \frac{P_{\text{grad}}\left(e_{\text{b}} - \frac{P_{\text{grad}} \cdot e_{\text{c}} \cdot L^2}{8(EI)_{\text{eff}}}\right)}{M_{\text{n,eff}}\left(1 - \frac{P_{\text{grad}}}{P_{\text{e,eff}}}\right)} = 1 \tag{2.9}$$

where : P_{grad} = the load capacity of column subjected to thermal gradient; $P_{\text{cr,eff}}$ =the load capacity of a hypothetical straight column that has same length, cross-section, and temperature distribution as the actual column, without including the effects of the second-order moments due to bowing or the shift in the effective centroid of the column; $M_{\text{n,eff}}$ = the nominal moment capacity of the column in the thermal gradient; $(EI)_{\text{eff}}$ = the elastic modulus of steel multiplied by the second moment of the effective area of the cross-section calculated about the neutral axis;

$$P_{\text{cr,eff}} = \begin{cases} \left[0.658^{\frac{P_{\text{y,eff}}}{P_{\text{e,eff}}}}\right] P_{\text{y,eff}}, & when P_{\text{e,eff}} \geq 0.44 P_{\text{y,eff}} \\ 0.877 P_{\text{e,eff}}, & when P_{\text{e,eff}} < 0.44 P_{\text{y,eff}} \end{cases} \tag{2.10}$$

Eq. (2.10), to be used for the calculation of $P_{\text{cr,eff}}$ is same as the AISC 360 column capacity equations for the flexural buckling limit state of a compression

member (E3-2 and E3-3) with the slight modifications. $P_{\mathrm{e,eff}}$ in Eq.(2.10) is the effective elastic buckling load.

$$M_{\mathrm{n,eff}} = \begin{cases} M_{\mathrm{p,eff}}, & \text{when H-W or } L < L_p \\ C_b\left[M_{\mathrm{p,eff}} - \left(M_{\mathrm{p,eff}} - 0.7F_{y,hot}S_{x,hot}\right)\left(\dfrac{L-L_p}{L_r-L_p}\right)\right] \le M_{\mathrm{p,eff}}, & \text{when } L_p \le L < L_r \text{ and H-S} \\ \dfrac{C_b\pi^2 E_{hot}}{\left(\dfrac{L}{r_t}\right)^2}\sqrt{1+0.078\dfrac{J}{S_{x,hot}h_0}\left(\dfrac{L}{r_t}\right)^2} \le M_{\mathrm{p,eff}}, & \text{when } L \ge L_r \text{ and H-S} \end{cases} \tag{2.11}$$

Where,

$$L_p = 1.1r_t\sqrt{\frac{E_{hot}}{F_{y,hot}}} \tag{2.12}$$

$$L_r = 1.95r_t\frac{E_{hot}}{0.7F_{y,hot}}\sqrt{\frac{J}{S_{x,hot}h_0}}\sqrt{1+\sqrt{1+6.76\left(\frac{0.7F_{y,hot}}{E_{hot}}\frac{S_{x,hot}h_0}{J}\right)^2}} \tag{2.13}$$

$$r_t = \frac{b_{f,\mathrm{hot}}}{\sqrt{12\left(1+\dfrac{h_c t_w}{6b_{f,\mathrm{hot}}t_{f,\mathrm{hot}}}\right)}} \tag{2.14}$$

$M_{\mathrm{n,eff}}$ is the nominal flexural capacity of the column in the direction of the thermal gradient with no axial load applied. It can be calculated by Eq. (2.11) based on the AISC flexural design provisions for asymmetric beam cross-sections.

Chapter 3. Heat Transfer Analysis

3.1 FE modeling

3.1.1 Modeling details

Before analysis of eccentricity, we decided that a FEM based software ABAQUS 2023 is used for the heat transfer analysis. And we assumed the real fire scenarios so that we can get *T-t* curve for design fire event through transient heat transfer analysis. For more accurate modeling and insulation, we selected solid, namely 20-node quadratic heat transfer brick heat transfer (DC3D20). Mesh size is 15~25mm across the section and 60~100mm along the length, two layers of meshes were placed in the through-thickness direction (Figure 3.1).

Part consists of H-400x400x13x21 and insulation. Temperature dependent thermal properties of H-shaped steel are taken as specified in the Eurocode-3 (EN 1993-1-2, 2005). In case of insulation, we used the stray-applied fire resistant material (SFRM) "CAFCO 300" from the previous study (Dwaikat et al., 2012). As prescribed by previous study (Dwaikat et al., 2012), Thickness of the insulation was 40mm in all sides for 2hr FRR (Fire Resistance Ratings). Thermal properties of the applied insulation are taken as specified in CAFCO 300.

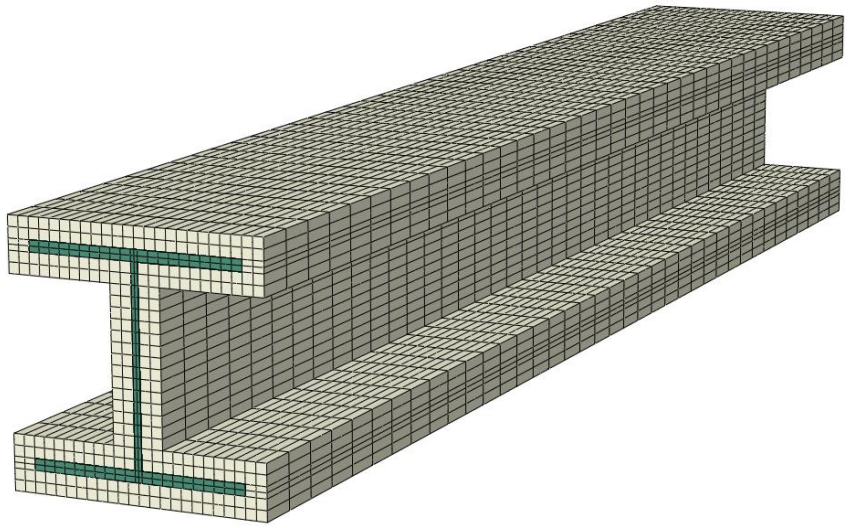

Figure 3.1 FE modeling of H-shaped steel and insulation

The heat transfer analysis accounts for heat transfer through convection and radiation between air and the exposed surface of the insulation or room temperature (20℃). For simulating the real fire scenario, we controlled the convection and radiation. A convection coefficient of 25 W/(m^2℃) was applied to the fire exposed surface of steel based on Eurocode-3 (EN 1993-1-2, 2005). A convection coefficient of 9 W/(m^2℃) was also applied to the surface in contact with room temperature. And the radiation was applied only the fire exposed surface. For the outer sides of flanges, the emissivity factor was 0.7 and for the internal side of flange and web, it was considered shadow effects. All of the specific values are shown in Figure 3.2. the Stefan-Boltzmann constant $\sigma = 5.6704 \times 10^{-8}\ W/m^2K$ was applied. We assumed that it is exposed by standard fire temperature-time curve from Eurocode-3 (EN 1993-1-2, 2005).

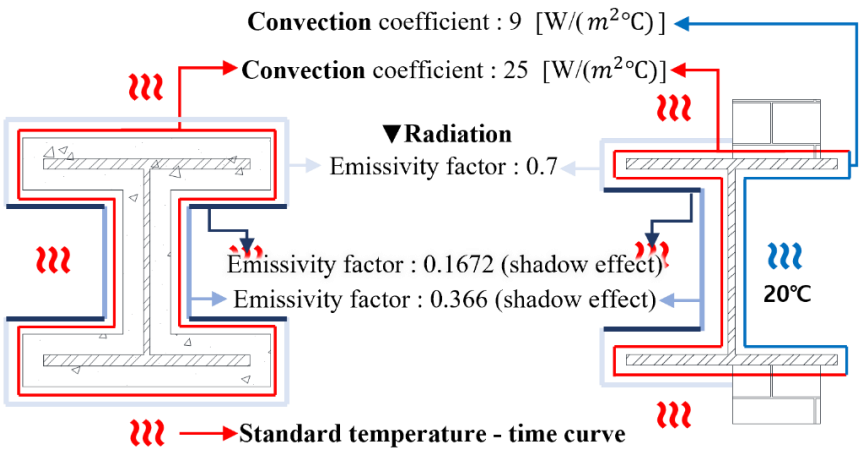

(a) Case of Insulation (b) Case of Insertion

Figure 3.2 FE modeling of H-shaped steel and insulation

3.2 Uniform and uneven heating conditions

We assumed 5 of real fire scenarios for obtaining thermal gradients. First, one side of insulation is detached at the end of fire protected steel. Second, 6% of insulation is detached at a distance 80mm from the end of insulation. Third, half of the steel with no insulation is inserted into the wall of a fire compartment and is exposed to room temperature. Forth, half of the steel is fully inserted into the wall of a fire compartment. In case of the last fire condition, one side of the steel inserted the wall is exposed fire and the other side is exposed room temperature. these 5 cases of real fire conditions can occur thermal gradients and we assumed that thermal gradients could occur along the flange (Figure 3.3 : ①~⑤) as well as along the web (Figure 3.4 : ⑥~⑩). In Figure 3.3 and Figure 3.4, the red wave means surfaces in fire and the blue means surfaces exposed room temperature. Furthermore, we conducted analysis of steel with uniform spray applied insulation.

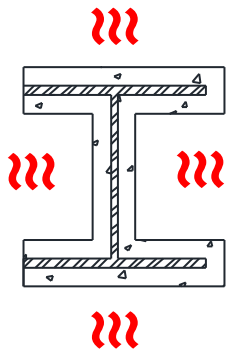	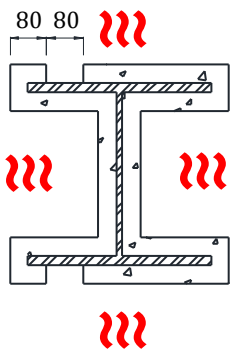	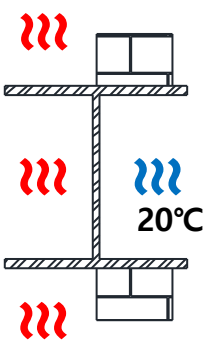
Case ①: Insulation detachment at end	Case ②: Partial detachment of insulation	Case ③: Partial insertion of steel into the wall

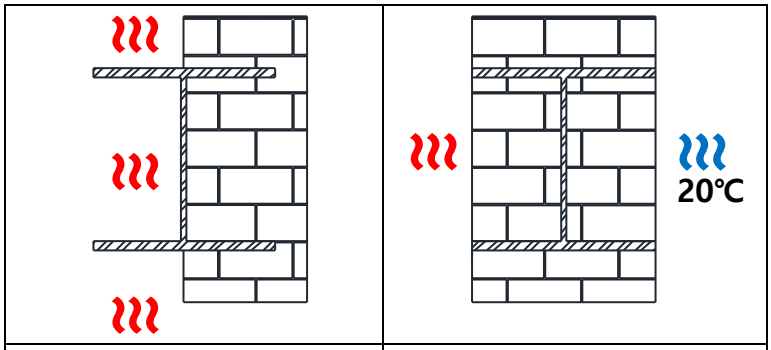

Case ④: Half insertion of steel into the wall	Case ⑤: All insertion of steel into the wall

Figure 3.3 Schematics of the heating configurations (H-W)

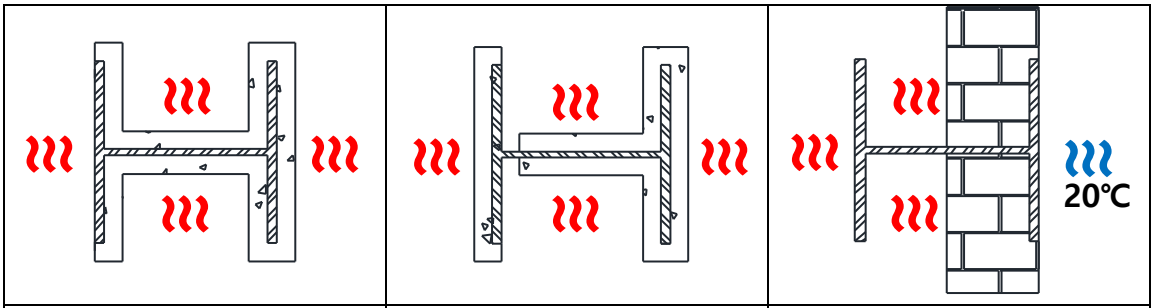

Case ⑥: Insulation detachment at end	Case ⑦: Partial detachment of insulation	Case ⑧: Partial insertion of steel into the wall

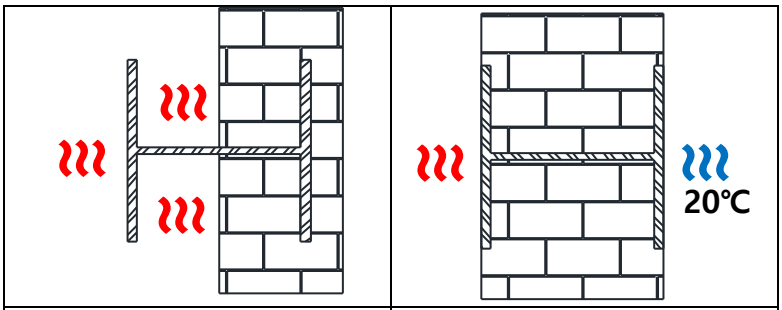

Case ⑨: Half insertion of steel into the wall	Case ⑩: All insertion of steel into the wall

Figure 3.4 Schematics of the heating configurations (H-S)

3.3 Result of heat transfer analysis

Through heat transfer analysis, the thermal gradient for each case can be obtained. Figure 3.5 and Figure 3.6 show the temperature distribution through a H-400x400x13x21 column cross-section. We can obtain maximum temperature and minimum temperature of thermal gradient from Figure 3.5 and Figure 3.6. Various types of thermal gradients are observed.

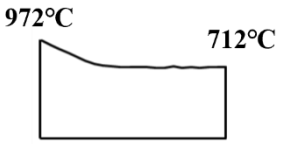	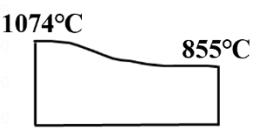	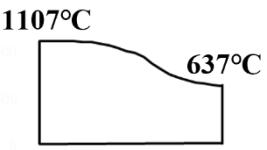
Case ①: Insulation detachment at end	Case ②: Partial detachment of insulation	Case ③: Partial insertion of steel into the wall

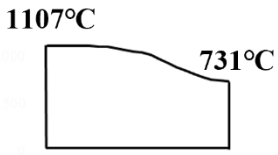	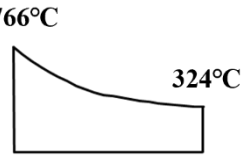
Case ④: Half insertion of steel into the wall	Case ⑤: All insertion of steel into the wall

Figure 3.5 Temperature distribution of cases at 3hr (H-W)

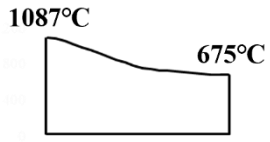	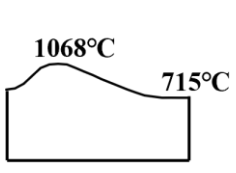	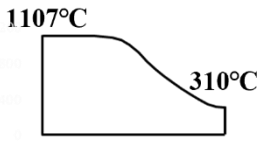
Case ⑥: Insulation detachment at end	Case ⑦: Partial detachment of insulation	Case ⑧: Partial insertion of steel into the wall

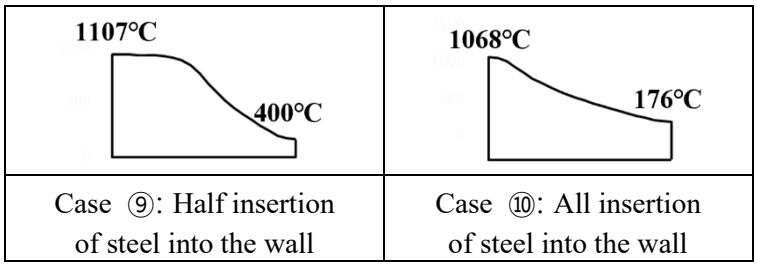

Case ⑨: Half insertion of steel into the wall	Case ⑩: All insertion of steel into the wall

Figure 3.6 Temperature distribution of cases at 3hr (H-S)

From the various thermal gradients, similar patterns can be classified together intuitively. As a result, it was possible to classify them into three main categories, and it could be simply schematized. Figure 3.7 shows the categorization into three groups and simple schematics of temperature distributions across the cross-section of steel from each group. As presented below, first simple schematic of thermal gradient is governed low temperature, second one is linear and third one is a type that high temperature is governing.

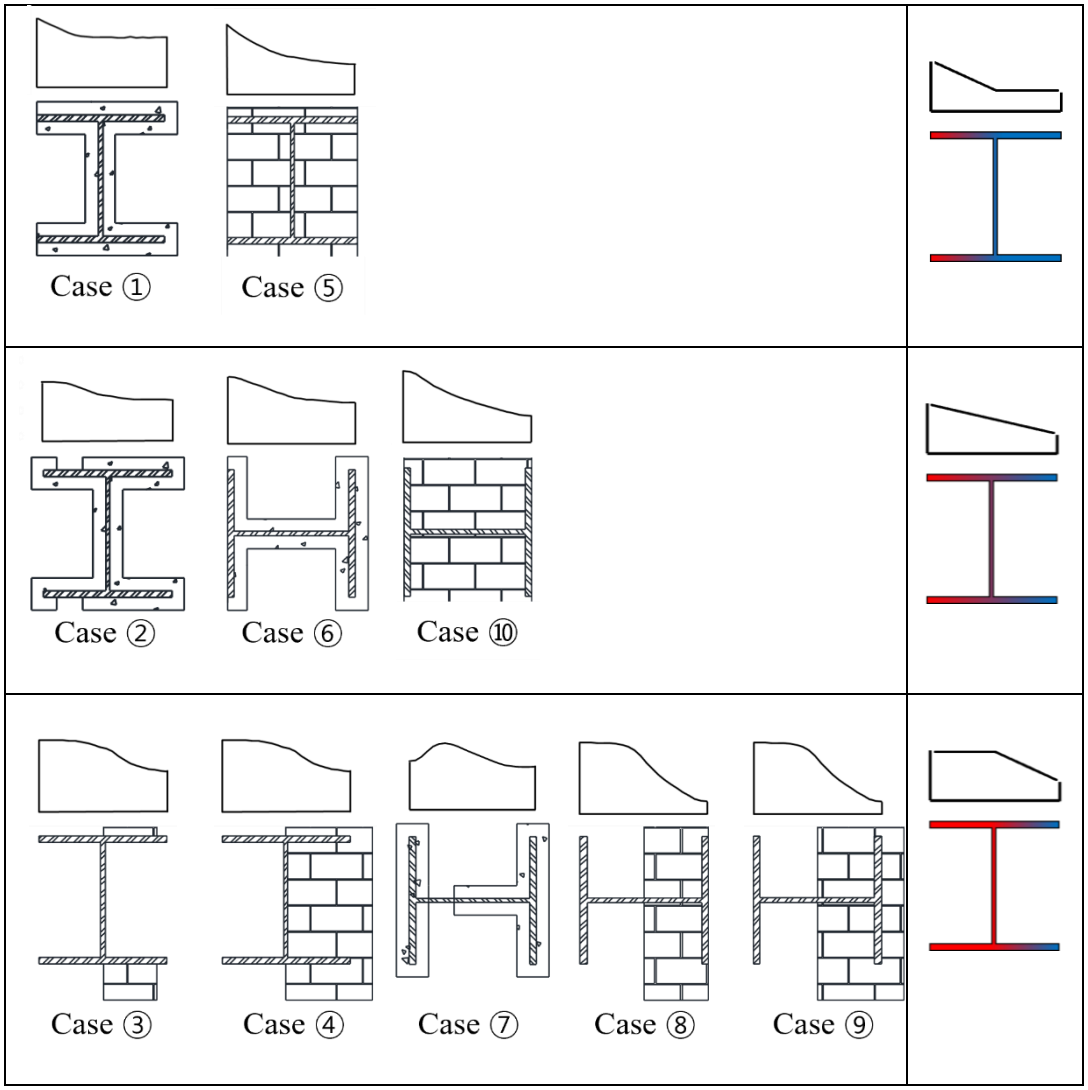

Figure 3.7 Classification and schematics of thermal gradients

Chapter 4. Calculation of Fire-Induced Eccentricity

As a temperature gradient develops, eccentricity over the cross-section occurs due to non-homogeneous fire properties etc. As mentioned above, eccentricity is caused by the shift of the stiffness center and thermal bowing. The eccentricity resulting from each factor can be theoretically determined based on mechanics of materials. This section analyzes the trends of the eccentricity, and proposes a simple equation for predicting the eccentricity with thermal gradients.

For the section condition, the study focused on the strong axis (H-S) and weak axis (H-W) of the H-shaped steel, which is the most commonly used type. A flange section was included, which is expected to occur eccentricity similar to that of the strong axis of the H-shaped steel. Additionally, the rectangular cross section was considered as well, which is anticipated to get results similar to the weak axis of the H-shaped steel. (Figure 4.1)

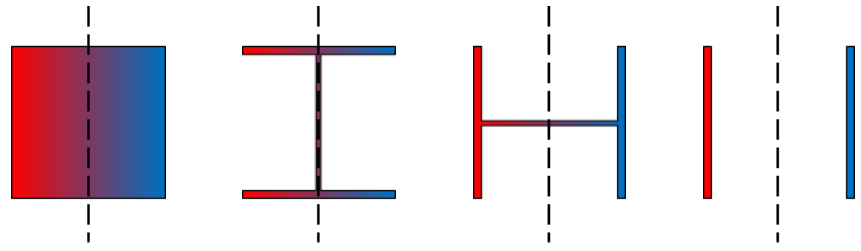

Figure 4.1 Type of section

Based on the results of the heat transfer analysis, thermal gradients were categorized into three types. These types include a linear thermal gradient, a "HIGH" thermal gradient dominated by high temperatures, which occurs due to fire exposure for a long time, and a "LOW" thermal gradient dominated by low temperatures, which usually occurs immediately after a fire. An additional thermal gradient "STEP" was considered. STEP induces the maximum shift in the center of stiffness. In the "HIGH" and "LOW" gradients, the bending point is at the center of the cross-section, while in the "STEP" gradient, the bending point is at the center of stiffness subjected to thermal gradients. Figure 4.2 shows the schematics of the thermal gradients.

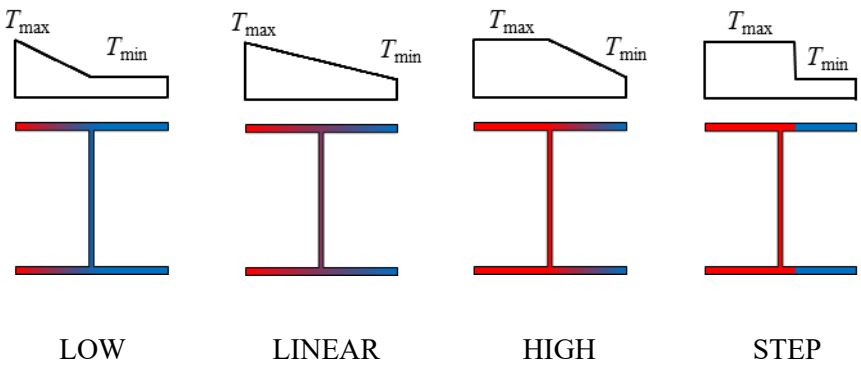

Figure 4.2 Schematics of the thermal gradients

4.1 Eccentricity due to stiffness center shift

When the steel is uniform section, the center of stiffness is determined solely by the shape of the cross-section. However, in non-uniform sections resulting from external factors such as temperature, the center of stiffness must be

determined by considering these factors. Steel has temperature-dependent properties. Consequently, the cooler side of the section has the higher stiffness, causing the center of stiffness to shift towards the cooler side. The stiffness at elevated temperature can be calculated by applying the reduction factor $k_{E,\theta}$ in Figure 4.3. Figure 4.4 shows stiffness distributions over the steel section for different thermal gradients. It is evident that each thermal gradient results in a different eccentricity.

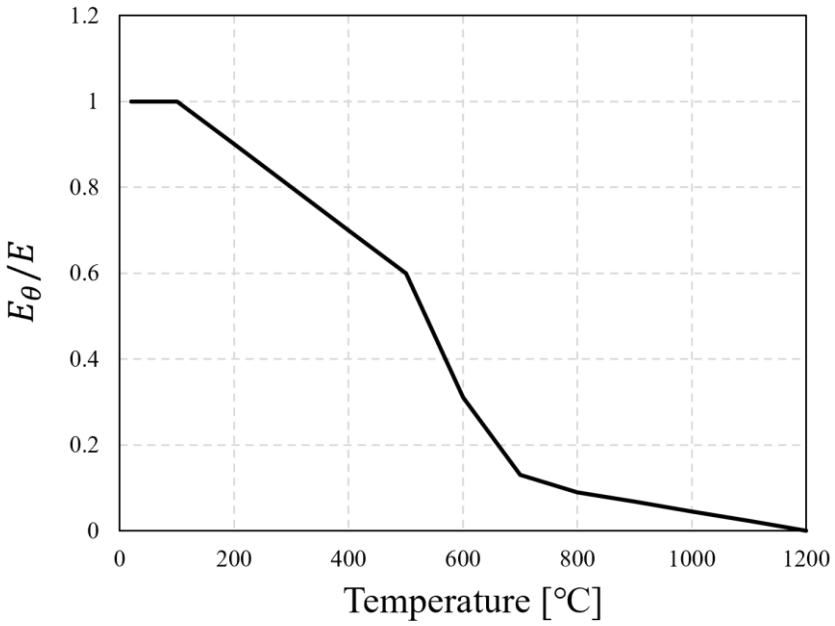

Figure 4.3 Reduction factor $k_{E,\theta}$ for the slope of the linear elastic range

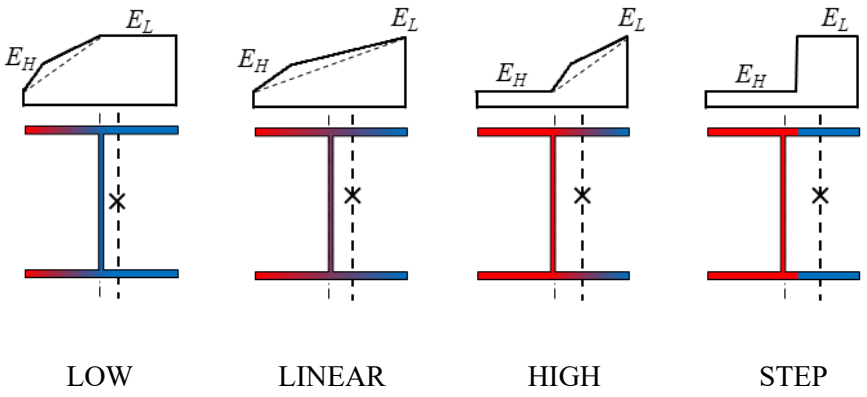

Figure 4.4 Stiffness distribution due to thermal gradients

When thermal gradients occur, the center of stiffness shifts due to the temperature-dependent stiffness. The displacement from the geometric centroid ($\bar{x}$) without a thermal gradient to the new center of stiffness (x_c) with a temperature gradient is referred to as the eccentricity due to the shift of stiffness center, denoted as e_c. In other words, the eccentricity (e_c) is obtained by subtracting the geometric centroid ($\bar{x}$) from the effective centroid (x_c).

In Figure 4.5, when the column is subjected to a uniform load, meaning that the axial load is applied at the geometric centroid. The shift of the effective centroid (e_c) induces the additional moment ($M = P \cdot e_c$) that causes the column to bend towards the cooler side. Therefore, it is necessary to calculate the eccentricity and consider the impact of the eccentricity on columns.

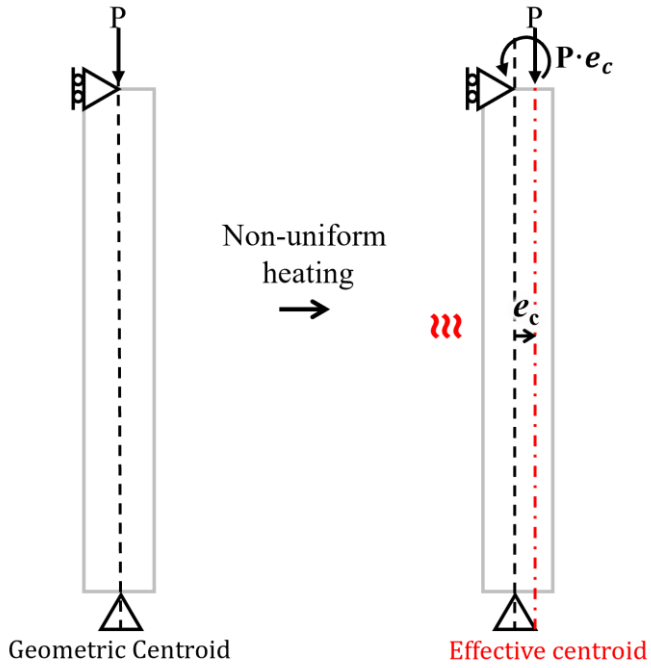

Figure 4.5 Shift of stiffness center

The eccentricity due to shift of the stiffness center can be calculated by Eq. (4.1).

$$\int_0^h xE(T)dA = \bar{x}\int_0^h E(T)dA \tag{4.1}$$

Where, x is start point of thermal gradient T is temperature $E(T)$ is temperature dependent elastic modulus.

To calculate the eccentricity using Eq. (4.1), it is necessary to define the stiffness equation $E(T)$ that varies with temperature. However, as shown in Figure 4.4, the stiffness equation $E(T)$ is relatively simply defined in the STEP gradient, which allows for theoretical calculations. Furthermore, as the

eccentricity with the STEP gradient is the upper bound, it is computed.

In a rectangular section, the eccentricity is calculated when a STEP temperature gradient occurs. Figure 4.6 shows the stiffness distribution for the STEP gradient and rectangular section. Where : E_H = the stiffness at the highest temperature in the STEP gradient; x_H = the distance that the highest temperature is distributed; E_L = the stiffness at the lowest temperature; x_L = the distance that the lowest temperature is distributed; b = the width of the section; h = the height of the section. The center of stiffness in rectangular section is $\bar{x}$. Therefore, substituting $E(T)$ into Eq. (4.1) provides the center of stiffness as Eq. (4.2) below.

$$\bar{x} = \frac{1}{2}\left\{ x_H + h + \frac{-h x_H E_H}{x_H (E_H - E_L) + h E_L} \right\} \tag{4.2}$$

The center of stiffness due to thermal gradient ($\bar{x}$) in the rectangular section can be obtained by substituting the value of x_H, which becomes zero when differentiated with respect to x_H. The maximum of the stiffness center ($\bar{x}_{max}$) can be obtained as shown in Eq. (4.3). The maximum eccentricity due to shift of stiffness center occurs when $\bar{x}$ and x_H are equal.

$$\bar{x}_{\max} = \frac{1}{1 + \sqrt{\frac{E_H}{E_L}}} h \tag{4.3}$$

The eccentricity is distance from geometric centroid, it can be calculated as Eq. (4.4).

$$(e_c)_{\substack{\text{RECT}\\\text{STEP}}} = \frac{1}{2}\cdot\frac{1-\sqrt{E_H/E_L}}{1+\sqrt{E_H/E_L}}h \tag{4.4}$$

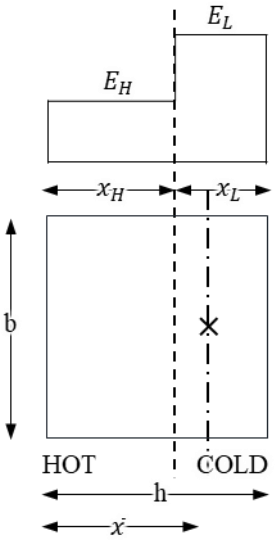

Figure 4.6 Stiffness center shift of rectangular by STEP gradient

When the STEP gradient occurs along the flange (H-W), the eccentricity can be calculated. The notation in Figure 4.7 is the same as that for the rectangular section (Figure 4.6). For the weak axis of the H-section, integration needs to be performed up to b instead of h for the center of stiffness ($\bar{x}$). Therefore, the center of stiffness in H-W (the weak axis of the H-section) is calculated as shown in Eq. (4.5) with b. Since the expression is complex, it was simplified using the A.

$$\bar{x} = \frac{1}{2}\left\{x_H + A + \frac{A(A-b)}{x_H - A}\right\} \tag{4.5}$$

$$\text{Where, } A = \frac{E_H t_w h' + 2bE_L t_f}{2(E_L - E_H)t_f}$$

The center of stiffness ($\bar{x}$) in H-W can be obtained by substituting the value of x_H, which becomes zero when differentiated by x_H, The maximum of the stiffness center ($\bar{x}_{max}$) can be obtained as shown in Eq. (4.6). The expression can be simplified by substituting *B*.

$$\bar{x}_{\max} = \frac{1}{1+\sqrt{\frac{B+E_H}{B+E_L}}} b \tag{4.6}$$

$$\text{Where, } B = \frac{t_w h'}{2t_f b} E_H$$

The maximum eccentricity due to shift of stiffness center occurs when $\bar{x}$ and x_H are equal.

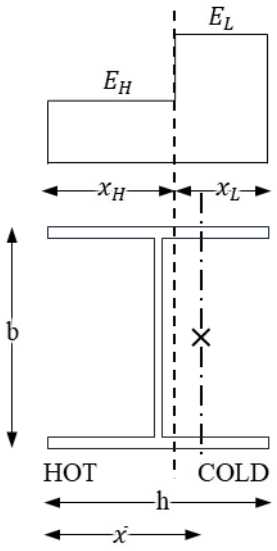

Figure 4.7 Stiffness center shift of H-W by STEP gradient

When the STEP gradient occurs along the web (H-S), the eccentricity was calculated. The notation in Figure 4.8 is the same as that for the rectangular section (Figure 4.6). The result of eccentricity calculation can be expressed by Eq. (4.7). For simplifying the equation, it is rearranged with *C, D.*

$$\bar{x} = \frac{1}{2}\left\{ x_H + C + \frac{C(C-b)}{x_H - D} \right\} \tag{4.7}$$

$$\text{Where,}\quad C = \frac{(E_L + E_H)b't_f + E_L h t_w}{(E_L - E_H)t_w}$$

$$D = \frac{-(E_L - E_H)b't_w{}^2 + h^2 t_w E_L + 2ht_f b' E_L}{(E_L + E_H)b't_f + E_L h t_w}$$

The maximum of the stiffness center ($\bar{x}_{max}$) in H-S can be obtained, as shown in Equation (4.8).

$$\bar{x}_{\max} = \frac{D/h}{1+\sqrt{1-\frac{D}{C}}}h \tag{4.8}$$

The maximum eccentricity due to shift of stiffness center occurs when $\bar{x}$ and x_H are equal.

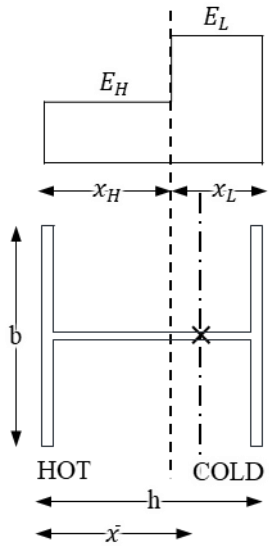

Figure 4.8 Stiffness center shift of H-S by STEP gradient

Lastly, the eccentricity due to the shift of the stiffness center was calculated for the STEP gradient in the FLANGE. The notation in Figure 4.9 is the same as that of the rectangular section (Figure 4.6). In FLANGE section, the highest and lowest temperatures are occurred at only both end flanges, respectively. It can be expected that the FLANGE is hardly affected by the thermal gradient. The center of stiffness in FLN is calculated as shown in Eq. (4.9). Assuming that the total cross-sectional area of a flange is *A* and each flange occupies half of the area, the equation can be simplified as shown in Eq. (4.9).

$$\bar{x} = \frac{1}{1+\frac{E_H}{E_L}} h \tag{4.9}$$

The eccentricity is distance from geometric centroid, it can be calculated as Eq. (4.10).

$$(e_c)_{\underset{0}{\text{FLN}}} = \frac{1}{2} \cdot \frac{1 - E_H / E_L}{1 + E_H / E_L} h \tag{4.10}$$

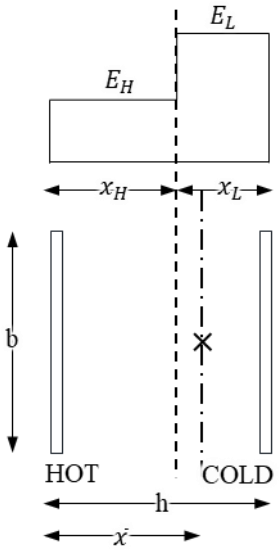

Figure 4.9 Stiffness center shift of FLANGE by STEP gradient

The eccentricity due to the shift of the stiffness center has been theoretically calculated for each section in the STEP gradient. The equation of eccentricity in the rectangular and flange section are organized in a relatively simple way, while H-sections (H-S, H-W) are more complex. However, predicting eccentricity for H-sections is crucial due to their wide uses. By utilizing the results from the rectangular section and flange section, it is possible to predict the eccentricity in H-sections.

Table 4.1 Summary of stiffness center shift by STEP gradient

RECTANGLE	H-W	H-S	FLANGE
$\bar{x}_{\max} = \frac{1}{1+\sqrt{\frac{E_H}{E_L}}} h$	$\bar{x}_{\max} = \frac{1}{1+\sqrt{\frac{B+E_H}{B+E_L}}} b$ $B = \frac{t_w h'}{2 t_f b} E_H$	$\bar{x}_{\max} = \frac{D/h}{1+\sqrt{1-\frac{D}{C}}} h$ $C = \frac{(E_L+E_H) b' t_f + E_L h t_w}{(E_L-E_H) t_w}$ $D = \frac{-(E_L-E_H) b' t_w^{\,2} + h^2 t_w E_L + 2 h t_f b' E_L}{(E_L+E_H) b' t_f + E_L h t_w}$	$\bar{x} = \frac{1}{1+\frac{E_H}{E_L}} h$

4.2 Eccentricity due to thermal bowing

Figure 4.10 shows the thermal bowing, where an uneven heating of the steel column causes significant expansion on the hotter side, resulting in bending of the column towards the hotter side. The eccentricity (e_b) represents the displacement due to thermal bowing from the geometric centroid. As a result of thermal bowing, the load, originally applied at the geometric centroid of the column, is now applied at a position as far away as the eccentricity (e_b). Consequently, the eccentric load induces an additional bending moment ($M = Pe_b$), which is a major factor in accelerating the buckling of the column. Therefore, it is essential to calculate the eccentricity due to thermal bowing and understand the effect of the eccentricity on the column.

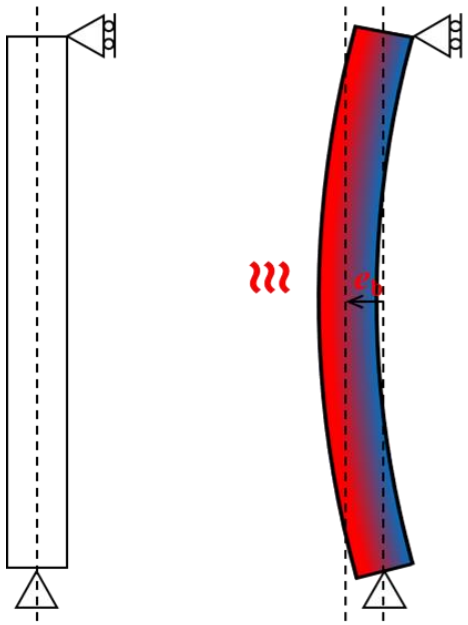

Figure 4.10 Thermal bowing

To theoretically calculate the eccentricity due to thermal bowing, it is necessary to assume that the column with non-uniform longitudinal temperature distribution can be neglected as mentioned section 2.2.2. Based on this assumption, the curvature of the column caused by thermal bowing maintains a constant value at all points of the column. When we define $u(x)$ as the equation of displacement with the vertical axis as the x-axis, the value obtained by differentiating $u(x)$ twice becomes the curvature of the column, φ_0. Therefore, Eq. (4.11) can be used to describe the curvature of the column.

$$u''(x) = -\varphi_0 \tag{4.11}$$

Since the curvature is a constant value, the equation of displacement $u(x)$ can be obtained by integrating $u''(x)$ twice. With the coordinates of $\left(\frac{L}{2}, 0\right)$ and $\left(-\frac{L}{2}, 0\right)$, which represent the supports of the column, the equation of displacement can be determined by eliminating the integration constant. This is expressed by Eq. (4.12).

$$u(x) = \frac{1}{2}\varphi_0\left[\left(\frac{L}{2}\right)^2 - x^2\right] \tag{4.12}$$

The maximum of eccentricity due to thermal bowing occurs at the center of the column, where $x = 0$. Therefore, the eccentricity due to thermal bowing can be calculated using Eq. (4.13).

$$e_b = \frac{1}{8}\varphi_0 L^2 \tag{4.13}$$

As shown in Eq. (4.13), the eccentricity due to thermal bowing is proportional to the curvature of the column when the column length (L) is constant. Therefore, it is crucial to calculate the curvature of the column theoretically.

In Figure 4.11, when a steel column is subjected to uneven heating, the strain due to thermal bowing occurs by the temperature as shown in Figure 4.12. It varies depending on the temperature. However, under the assumption of Euler-Bernoulli beam theory that the cross-section remains flat, the actual strain can be expressed as linear. The actual strain can be expressed as a linear function passing through a specific point, as shown in Eq. (4.14).

$$\varepsilon(x) = -\varphi_0 (x - x_c) + \varepsilon_0 \tag{4.14}$$

Where, x_c is the center of stiffness subjected to thermal gradient, ε_0 is the strain at x_c.

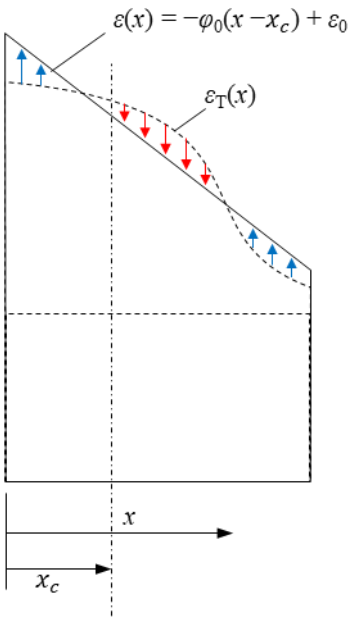

Figure 4.11 Difference of strain due to thermal bowing

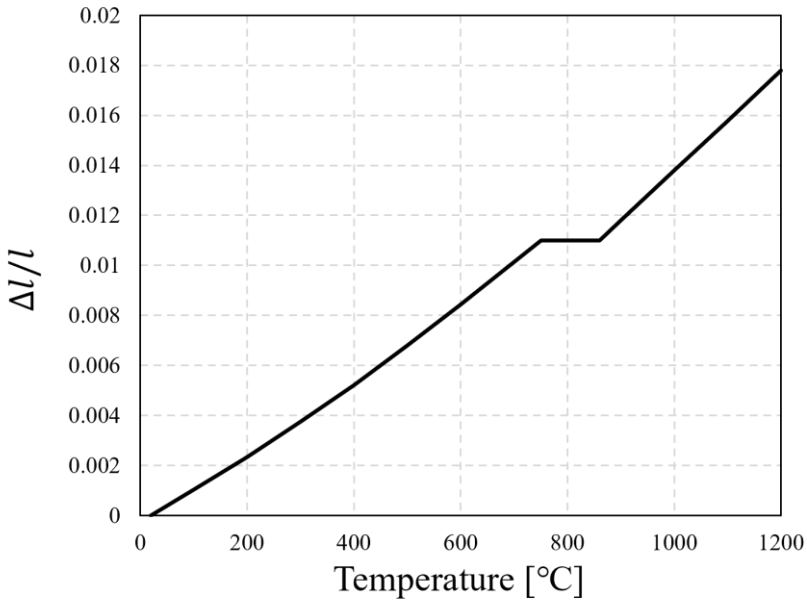

Figure 4.12 Relative thermal elongation of carbon steel as a function of the temperature

As shown in Figure 4.11, a difference between the strain due to thermal bowing $\varepsilon_T(x)$ and the actual strain $\varepsilon(x)$ occurs because the strain due to thermal bowing must maintain a flat shape according to the Bernoulli-Euler beam assumption. The difference induces stress $\sigma(x)=E(x)\left(\varepsilon(x)-\varepsilon_T(x)\right)$ across the section, and Eqs. (4.15) and (4.16) can be set up to satisfy self-equilibrium.

$$P=\iint_A \sigma(x)dA=0 \tag{4.15}$$

$$M=\iint_A \left(x-x_c\right)\sigma(x)dA=0 \tag{4.16}$$

ε_0 can be obtained from Eq. (4.17), and φ_0 can be obtained from Eq. (4.18).

$$\varepsilon_0=\frac{\int_0^h \varepsilon_T(x)E(T)b(x)dx}{\int_0^h E(T)b(x)dx} \tag{4.17}$$

$$\varphi_0=\frac{\int_0^h (x-x_c)\varepsilon_T(x)E(T)b(x)dx}{\int_0^h (x-x_c)^2 E(T)b(x)dx} \tag{4.18}$$

The curvature is determined by Eq. (4.18) with the strain by thermal bowing and the stiffness equation. The stiffness equation can be calculated by considering the reduction factor $k_{E,\theta}$ as shown in Figure 4.3, while the strain due to thermal bowing $\varepsilon_T(x)$ can be obtained using Figure 4.12.

In the case of a LINEAR thermal gradient, as the strain due to thermal bowing $\varepsilon_T(x)$ occurs linearly, As a results, there is no difference between the

actual strain $\varepsilon(x)$ and the strain due to thermal bowing $\varepsilon_T(x)$. Consequently, under the LINEAR temperature gradient, the curvature $\underset{0}{\varphi}_{\text{LINEAR}}$ can be easily obtained from Eq. (4.19).

$$\underset{0}{\varphi}_{\text{LINEAR}} = \frac{1}{h}\left(\varepsilon_{\text{H}} - \varepsilon_{\text{L}}\right) \tag{4.19}$$

Where, ε_{H} is the strain at the highest temperature, ε_{L} is strain at the lowest temperature.

In STEP gradient, the curvature due to thermal bowing can be calculated with hand due to simple stiffness equation $E(T)$. As a result of calculation by applying a simple stiffness equation $E(T)$ to Eq.(4.18), Eq.(4.20) can be obtained.

$$\underset{\text{RECT}}{\varphi}_{\text{STEP}} = \frac{3}{2h}\left(\frac{\varepsilon_{\text{T,H}} E_{\text{H}} F^2 - \varepsilon_{\text{T,L}} E_{\text{L}} (1-F)^2}{E_{\text{H}} F^3 + E_{\text{L}} (1-F)^3}\right) \tag{4.20}$$

$$\text{Where, } F = \frac{1}{1+\sqrt{\frac{E_H}{E_L}}}$$

For thermal gradient conditions other than LINEAR and STEP, the change of stiffness due to temperature becomes irregular and complex, making it difficult to approach theoretically. Numerical methods are often employed in such cases. Hence, the prediction of eccentricity due to thermal bowing in each section under different thermal gradients can be achieved by utilizing the LINEAR gradient that can be calculated most easy.

4.3 Calculation of eccentricity under thermal gradient

4.3.1 Eccentricity of stiffness center shift

All the eccentricity equations for the shift of the stiffness center can be expressed in the cross-section where the thermal gradient occurs, namely the height (h) or width (b) of the section (Table 4.1). To evaluate the effect of eccentricity independent of the section size, the eccentricity was normalized by dividing them by h or b, and analyzed as non-dimensional values.

In cross-sections, the study focused on the rectangular section, flange section, and the weak and strong axes of the H-shaped steel. For the H-section, three wide sections were considered: H-400x400x13x21, H-300x300x10x15, and H-200x200x8x12, and three narrow section: H-400x200x8x13, H-300x150x6.5x9, and H-200x100x5.5x8. Total 14 types of sections were considered.

To examine the effect of section size, the eccentricity was compared between three wide sections (H-400x400x13x21, H-300x300x10x15, and H-200x200x8x12) and three narrow sections (H-400x200x8x13, H-300x150x6.5x9, and H-200x100x5.5x8) in various temperature conditions. The results showed that both wide and narrow sections were not significantly affected by the section size. Furthermore, there was a slight difference between the wide and narrow sections, it was negligible. As narrow sections are not commonly used, the H-400x400x13x21 (wide section) was chosen when calculating the eccentricity. Therefore, in the analysis of eccentricity, four types of cross-section were considered: rectangular, flange, and H-400x400x13x21 (strong axis, weak axis).

The combinations of temperatures (20℃, 100℃, 200℃, 300℃, 400℃, 500℃, 600℃) result in 27 temperature combinations, and 4 types of thermal gradients are assumed. Calculations were performed for 108 temperature conditions. However, since the stiffness is the same at 20℃ and 100℃, these temperature combinations were not included. Consequently, considering the section conditions, the eccentricity due to the shift of the stiffness center was calculated for a total of 1,512 cases.

To analysis the trends of the eccentricity under different conditions, the eccentricity was compared when the lowest temperature of 200℃ and the highest temperature of 600℃ are fixed in Figure 4.13. In section conditions, the FLANGE section consistently occurs the largest eccentricity. Additionally, the eccentricity occurred in the following order: H-section with strong axis, rectangular section, and H-section with weak axis. In the case of the H-section with strong axis, the trend can be observed as a combination of the flange and rectangular cross-section trends. Moreover, for the H-section with weak axis, it follows closely the trend of the rectangular section.

Compared with temperature distribution, the maximum eccentricity was observed in the STEP thermal gradient, followed by HIGH, LINEAR, and LOW in decreasing order. The FLANGE section showed the same eccentricity regardless thermal gradients.

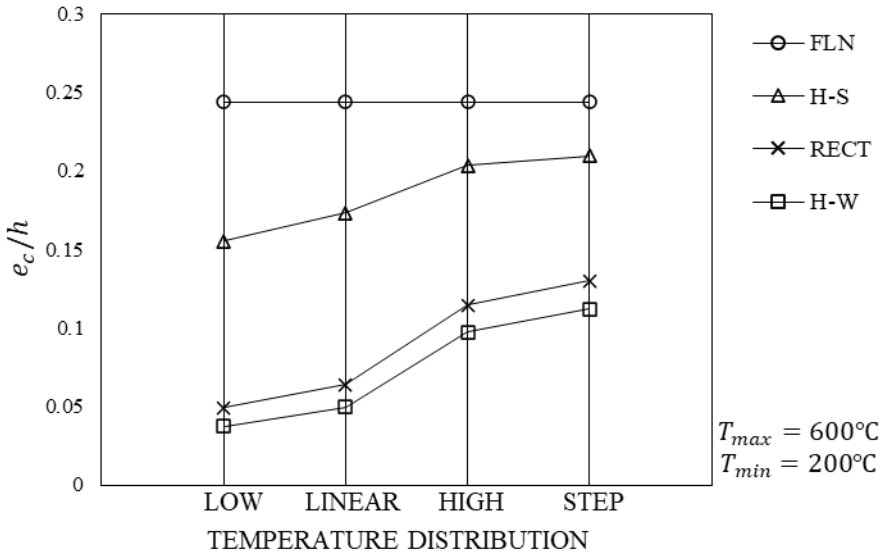

Figure 4.13 e_c / h with different sections and temperature distributions

4.3.2 Eccentricity of thermal bowing

As shown in Figure 4.14, the curvature caused by thermal bowing is inversely proportional to the height (h) of the section when the same thermal gradients occur. This principle is similar to the concept that in a curve, as the radius of curvature increases, the curvature becomes flat. In this study, it was determined to compare the curvature, which solely reflects the impact of the thermal gradient, by multiplying it with the height (h) of the cross-section, regardless of the section size.

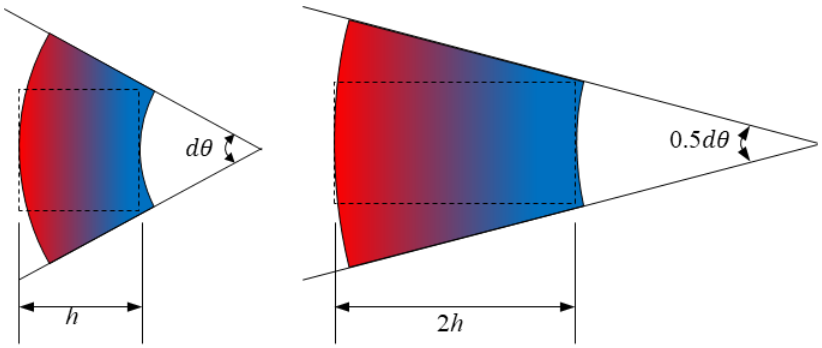

Figure 4.14 Effect of width of section on curvature

The section and temperature conditions were the same as when calculating the eccentricity due to the shift of the stiffness center. Therefore, four types of cross-sections (RECT, H-S, H-W, FLN) were considered, and only the wide section was taken into account since there was no difference between narrow and wide sections. The temperature combinations ranged from 20°C to 700°C, and since there was no stiffness difference between 20°C and 100°C, these two combinations were not included. Total temperature combinations result in 27. Considering four types of temperature gradients (LOW, LINEAR, HIGH, STEP), the eccentricity due to thermal bowing was calculated in 432 cases.

In Figure 4.15, The eccentricity was analyzed with the maximum temperature of 600°C and the minimum temperature of 200°C, similar to the eccentricity due to the shift of the stiffness center. All LINEAR gradients calculated the same eccentricity value regardless of the cross-section types. All FLANGE sections also calculated the same regardless of the thermal gradients. In the STEP and HIGH gradients, the H-section with weak axis calculated the highest eccentricity, followed by the rectangular section, the H-section with strong axis, and the FLANGE. Furthermore, the STEP temperature gradient still

resulted in the largest eccentricity for each section.

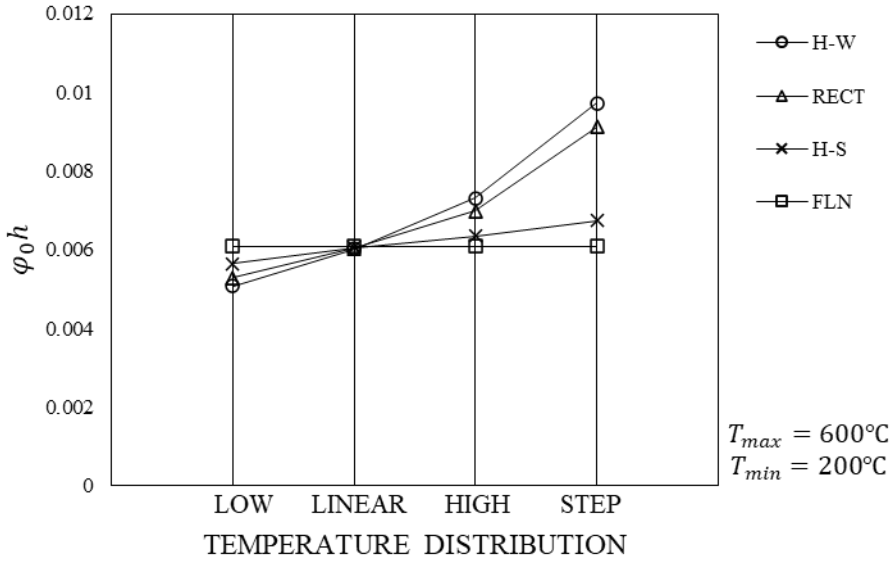

Figure 4.15 $\varphi_0 \cdot h$ with different sections and temperature distributions

4.4 Simple formula for fire-induced eccentricity of H-shape steel columns

As mentioned above, the eccentricity caused by the thermal gradient has a negative effect on the column, it is necessary to calculate the eccentricity and consider its effects in design. However, calculation of the eccentricity in H-shaped section is highly complex and time-consuming. Therefore, by utilizing equations that can be obtained simply, the eccentricity under each condition can be predicted.

4.4.1 Shift of stiffness center

In the case of eccentricity due to the shift of the stiffness center, it can be observed in Figure 4.13 that the eccentricity of the H-section can be predicted by combining the eccentricity of the flange and rectangular sections. From Table 4.1, the equations for the eccentricity of the rectangular section and the flange can be calculated theoretically under the STEP temperature gradient. Therefore, using Equation (4.21), the eccentricity of the H-sections was predicted using eccentricity of the flange and rectangular sections. The eccentricity of the two cross sections is multiplied by the coefficients *a* and *b* to predict the eccentricity of the other cross section.

$$(e_c)_{\underset{temp}{section}} = a_{section}(e_c)_{\underset{0}{\mathrm{FLN}}} + b_{section}(e_c)_{\underset{temp}{\mathrm{RECT}}} \tag{4.21}$$

The coefficient d_{temp} is added for reflecting impact of the thermal gradients.

The FLANGE section is regardless the thermal gradient, no coefficient d_{temp} is required. The effect of the thermal gradient is reflected by multiplying the eccentricity due to the rectangular section by the coefficient, as shown in Equation (4.22).

$$\left(e_c\right)_{\substack{\text{RECT}\\temp}} = d_{temp}\left(e_c\right)_{\substack{\text{RECT}\\\text{STEP}}} \tag{4.22}$$

$$\left(e_c\right)_{\substack{\text{section}\\temp}} = a_{\text{section}}\left(e_c\right)_{\substack{\text{FLN}\\0}} + b_{\text{section}}d_{temp}\left(e_c\right)_{\substack{\text{RECT}\\\text{STEP}}} \tag{4.23}$$

To consider the effect of the thermal gradient, relationship between the eccentricity of each thermal gradient and the eccentricity of the STEP thermal gradient in the rectangular section was analyzed, as shown in Figure 4.16. The slope of LOW was determined to be 0.8895 with R^2 of 0.9975, indicating a reliable trend. Similarly, the slope of LINEAR was calculated as 0.5296 with R^2 of 0.9821, while the slope of HIGH was 0.3781 with R^2 of 0.9567. The slope represents the ratio of the eccentricity in the rectangular section under each thermal gradient to the eccentricity in the rectangular section under the STEP temperature gradient, serving as a coefficient that accounts for the influence of the temperature gradient. Consequently, the coefficient can be summarized in Table 4.2, displayed with two decimal places.

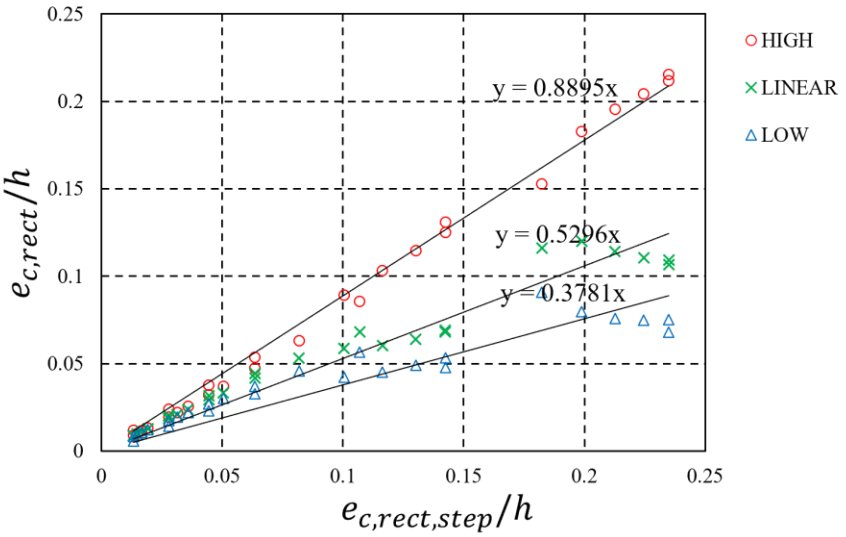

Figure 4.16 The ratio of $(e_c)_{\substack{\text{RECT}\\temp}}$ to $(e_c)_{\substack{\text{RECT}\\\text{STEP}}}$ for d_{temp}

Table 4.2 Correction factor d_{temp} for each temperature gradient

d_{STEP}	1.00
d_{HIGH}	0.89
d_{LIN}	0.53
d_{LOW}	0.38

The coefficients, which account for the impact of the temperature gradient, have been determined, and an analysis has been conducted on the coefficients $a_{section}$ and $b_{section}$, which represent the influence of the cross section. The coefficient $a_{section}$ indicates the contribution of the flange section to the target section by multiplying the eccentricity of the flange section, while the coefficient $b_{section}$ represents the contribution of the rectangular section to the target section by multiplying the eccentricity of the rectangular section.

For the FLANGE section, the coefficient $a_{section}$ is 1 and the coefficient $b_{section}$ is 0. Conversely, for a rectangular cross section, the coefficient $b_{section}$ is 1 and the coefficient $a_{section}$ is 0. In the case of an H-section, which combines both the flange and rectangular sections, the most suitable values for $a_{section}$ and $b_{section}$ were determined by substituting numbers between 0 and 1. For all combinations of $a_{section}$ and $b_{section}$, graphs were plotted to compare the actual values with the values obtained using the proposed equation, and the coefficients that R^2 is closest to 1 were adopted. The results are shown in Table 4.3.

Table 4.3 Correction factor $a_{section}$ and $b_{section}$ for each section

	$a_{section}$	$b_{section}$
FLANGE	1.0	0.0
H-S	0.5	0.7
RECTANGULAR	0.0	1.0
H-W	0.0	0.9

When comparing the actual eccentricity using the heat transfer analysis and the predicted value with the proposed equation, it can be concluded that the proposed equation predicts the eccentricity well, as shown in Figure 4.17. When comparing the actual eccentricity using the heat transfer analysis and the upper limit with the proposed equation, it was found that none of the results exceeded the upper limit.

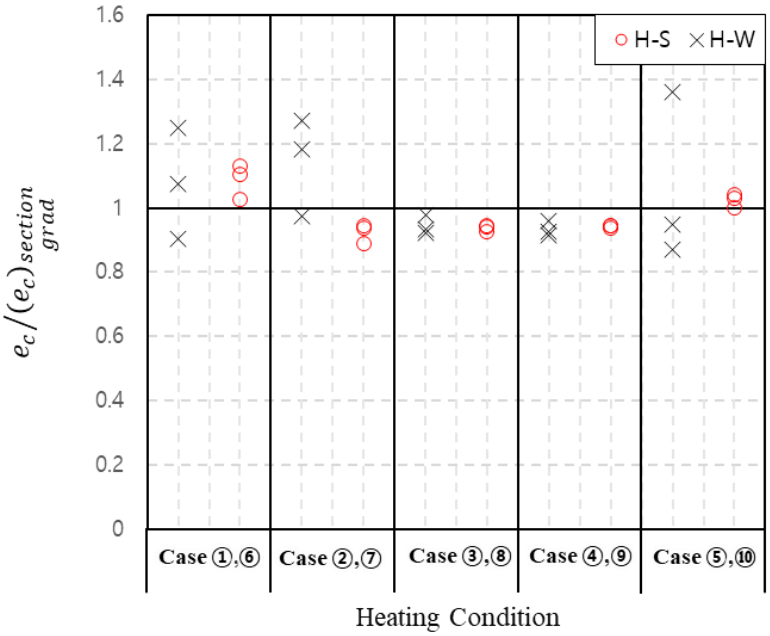

Figure 4.17 Validation of the proposed equation for e_c

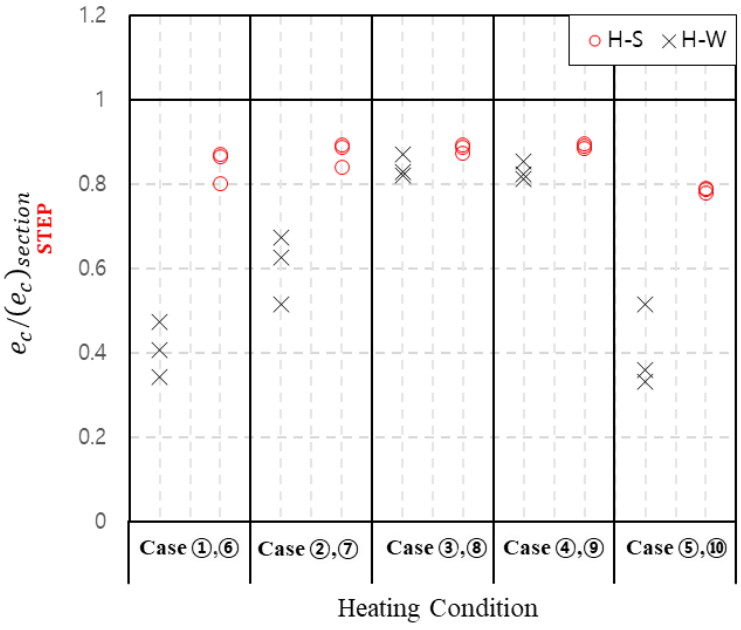

Figure 4.18 Validation of the upper limit for e_c

4.4.2 Thermal bowing

In the eccentricity due to thermal bowing, Figure 4.15 demonstrates that the eccentricity in the LINEAR temperature gradient is calculated the same regardless of the cross section. Similarly, the eccentricity for the flange remains constant regardless of the thermal gradient. Overall, the eccentricity shows a reversed trend based on the eccentricity in FLN and LIN, gradually increasing for each section. It's important to note that the x-axis in the graph does not have a numerical meaning but just for categorization of thermal gradients, so the intervals do not need to be same. By adjusting the x-coordinate and expressing it as a linearly increasing form, the eccentricity for each condition can be predicted. For the linear expression, a straight line passing through the FLN and LIN coordinates $\left(x_{\mathrm{LIN}}, y_{\substack{\mathrm{FLN} \\ \mathrm{LIN}}} \right)$ can be assumed as expressed in Eq. (4.24).

$$y_{\substack{section \\ temp}} = m_{section}(x_{temp} - x_{\mathrm{LIN}}) + y_{\substack{\mathrm{FLN} \\ \mathrm{LIN}}} \tag{4.24}$$

Where, $m_{section}$ is the slope that varies according to the cross section, x_{temp} is the x-coordinate that changes with the thermal gradient.

Figure 4.15 shows the constant curvature of the FLANGE section in the LINEAR temperature gradient due to the FLANGE maintaining a constant value regardless of the temperature gradient, and the LINEAR temperature gradient having same value regardless of the cross section. Hence, the eccentricity due to the thermal bowing can be predicted using a linear equation passing through a point $\left(0, (\varphi_0)_{\substack{\mathrm{FLN} \\ \mathrm{LIN}}} \right)$.

Figure 4.19 is expressed as a linear graph by adjusting the x-coordinate. This linear equation corresponds to Eq. (4.24), where $c_{section}$ is substituted as the slope value reflecting the effect of the section, and the influence of thermal gradients is represented by f_{temp}. It can be rearrange as shown Eq. (4.25).

$$\left(\varphi_0\right)_{\substack{section \\ temp}} = \left(c_{section}\, f_{temp} + 1\right) \cdot \left(\varphi_0\right)_{\substack{FLN \\ LIN}} \tag{4.25}$$

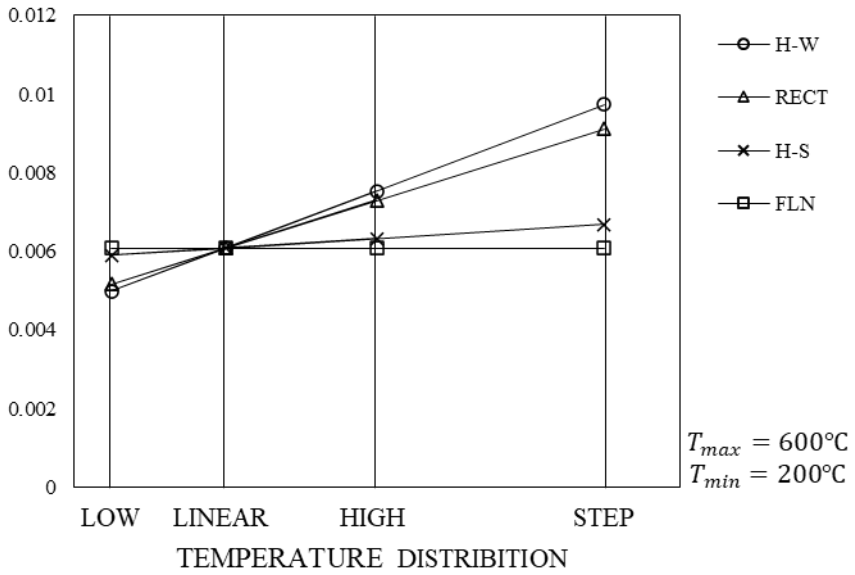

Figure 4.19 $\varphi_0 \cdot h$ with different sections and temperature distributions modified for straight line

Table 4.4 shows the specific values of $c_{section}$ and f_{temp}.

Table 4.4 Correction factor $c_{section}$ and f_{temp} for each section

	$c_{section}$	f_{temp}
FLANGE/ STEP	0.0	0.0
H-S/ HIGH	0.1	0.4
RECTANGLE/ LINEAR	0.5	-0.3
H-W/ LOW	0.6	1.0

When the coefficient $c_{section}$ reflecting the section becomes zero, the curvature of the flange φ_0 can be determined. It means the flange is independent of the temperature gradient and $(\varphi_0)_{\underset{temp}{\text{FLN}}} = (\varphi_0)_{\underset{\text{LIN}}{\text{FLN}}}$. Similarly, the curvature in the LINEAR temperature gradient can be obtained by substituting zero for the coefficient reflecting the effect of the temperature gradient f_{temp}.

When comparing the actual eccentricity using the heat transfer analysis and the predicted value with the proposed equation, it can be concluded that the proposed equation predicts the eccentricity well. When comparing the actual eccentricity using the heat transfer analysis and upper limit of the proposed equation, it was found that the results don't exceed the upper limit unreasonably.

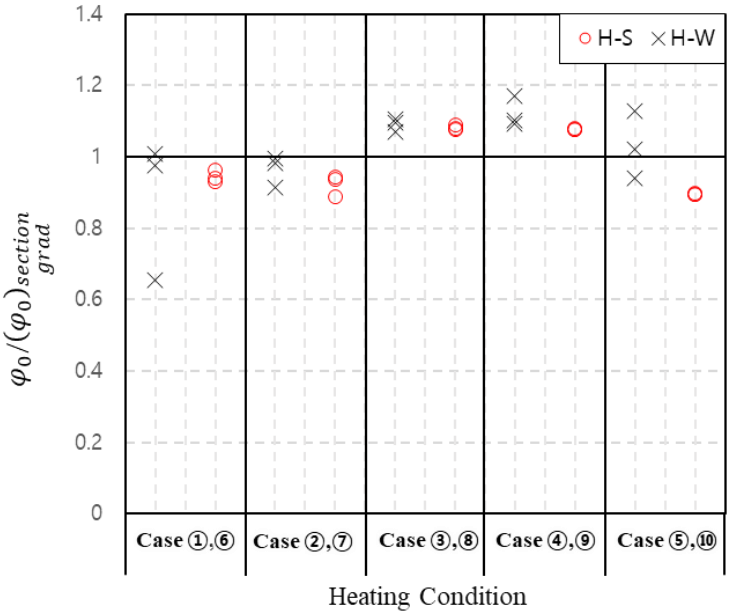

Figure 4.20 Validation of the proposed equation for φ_0

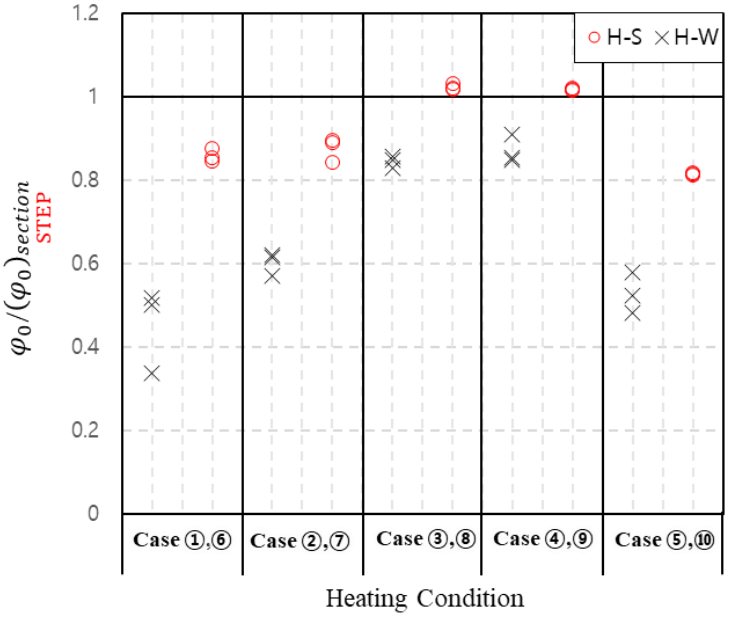

Figure 4.21 Validation of the upper limit for φ_0

Chapter 5. Effects of Eccentricity on Fire Resistance

5.1 Finite element modeling

A numerical investigation was conducted to examine the effect of thermal gradient on the column when it is unevenly heated. The investigation utilized finite element (FE) analysis with the commercial software ABAQUS 2023. The 20-node solid elements with reduced integration (C3D20R in ABAQUS) was chosen as the element type. The column length was set to 3m, 5m, and 7m, with an H-400x400x13x21 cross-section. The load ratio was varied between 0.3, 0.4, 0.5, 0.6, and 0.7. An initial imperfection of $L/1000$ was applied, and a simple supported condition (pin-roller) was used as the boundary condition. As mentioned in section 2.2.3, previous experimental studies confirmed the release of residual stresses in steel columns at high temperatures. Therefore, the FE analysis was conducted without considering residual stresses.

Table 5.1 Abaqus modeling detail

Cross-section	H-400x400x13x21
Element type	C3D20R A 20-node quadratic brick, reduced integration. 3D Stress
Mesh size	across the section: 15~25mm along the length: 60~100mm
Column length	3m, 5m, 7m
Load ratio	$P = (0.3, 0.4, 0.5, 0.6, 0.7) \times F_y A$
• Temperature-time relationship from previous heat transfer analysis in Ch. 4 were assigned. • Initial imperfection and geometric nonlinearity were considered. • *Euler* column (simply supported condition) was used. • Based on the previous studies showing that residual stresses are released at elevated temperatures, we neglected the residual stresses.	

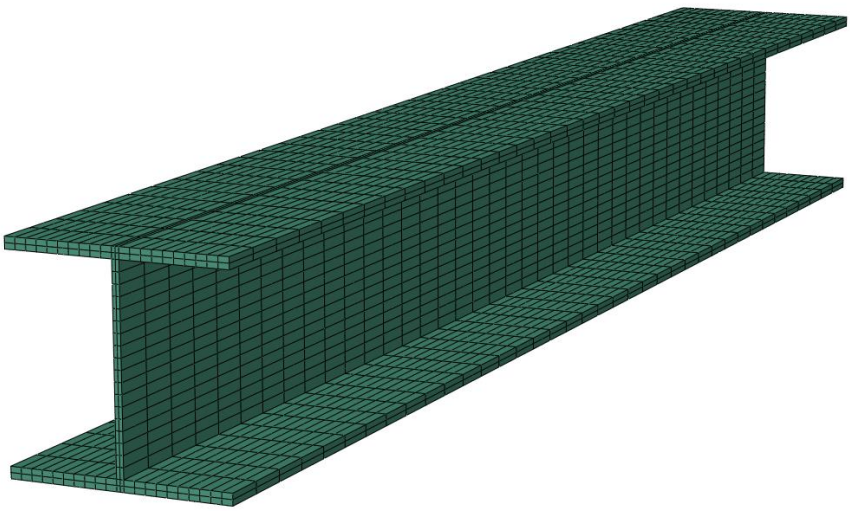

Figure 5.1 FE modeling of H-shaped steel

In Figure 5.2, The analysis method for load heat analysis is shown. Initially,

a load *P* is applied to the column using a ramp function. Temperature-time data is then extracted for each node from the heat transfer analysis results. This data is directly mapped onto the column to which the load was applied, resulting in the heating of the column.

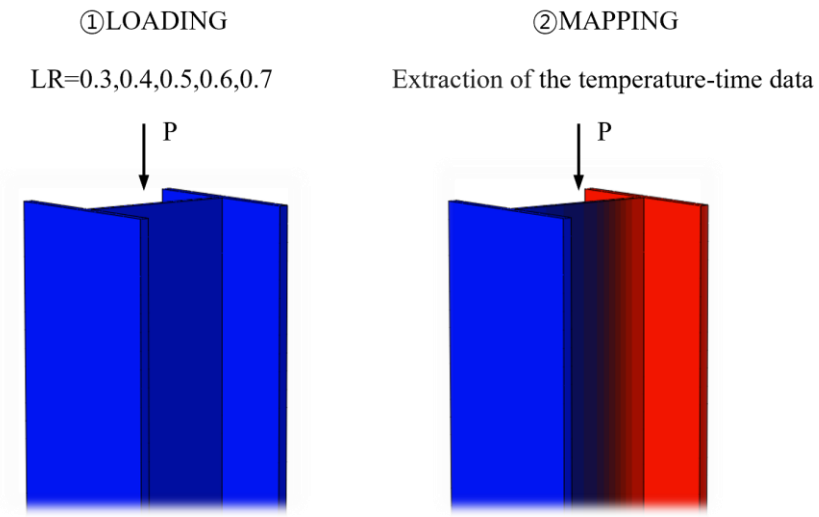

Figure 5.2 FE analysis method

5.2 Effects on fire resistance time and load bearing capacity

As described in section 2.1 above, it is specified to neglect non-uniform heating conditions in the design because uniformly heated columns reach their failure temperature faster than non-uniformly heated columns in AISC 360-22. This is based on the research conducted by Agarwal et al. (2014) Figure 5.3 shows the displacement-time relationship of (a) Thermal gradient along the flange (H-S) and (b) Thermal gradient along the web (H-W). For a column length of 3m and a load ratio of 0.5, six different cases were compared, including five fire conditions in the heat transfer analysis and the case of UNIFORM, which is insulated from all sides. AISC 360-22 only considers cases where thermal gradients occurred by a low heat influx. However, when considering various fire scenarios inducing thermal gradients, such as insulation detachment, it can be confirmed that the failure temperature for each case varies significantly. As mentioned in AISC 360-22, case 5 has a very long fire resistance time of 169 minutes due to low heat influx. On the other hand, in cases 2 and 7, despite partial insulation detachment, the fire resistance time is reduced by approximately 90 minutes compared to UNIFORM with full insulation. This indicates that even a small insulation loss has a significant impact on the fire resistance time of the column. Since thermal gradients can occur under more diverse conditions in reality than the five cases presented in this study, it cannot be assured that situations with thermal gradients are structurally safer. As the results, the effect of thermal gradient should not be neglected.

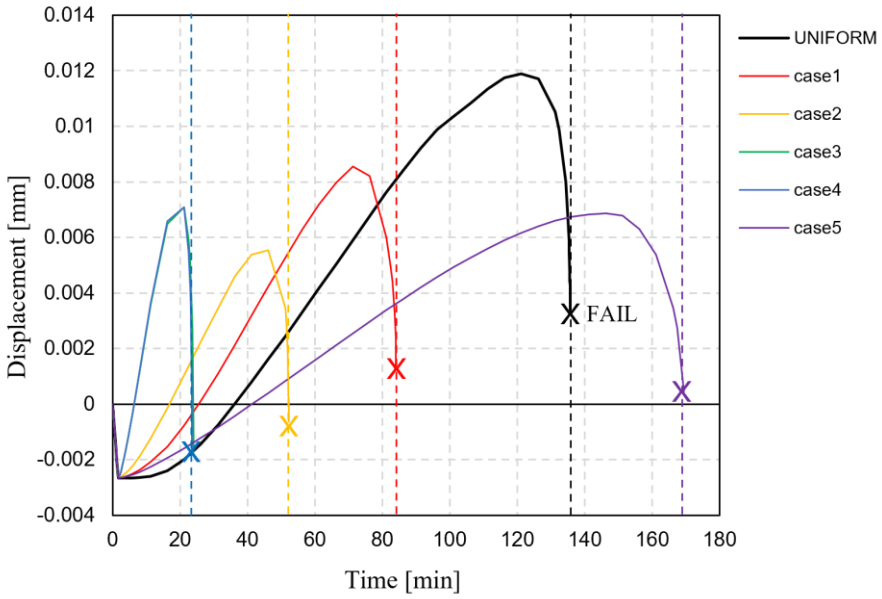

(a) Thermal gradient along the flange (H-W)

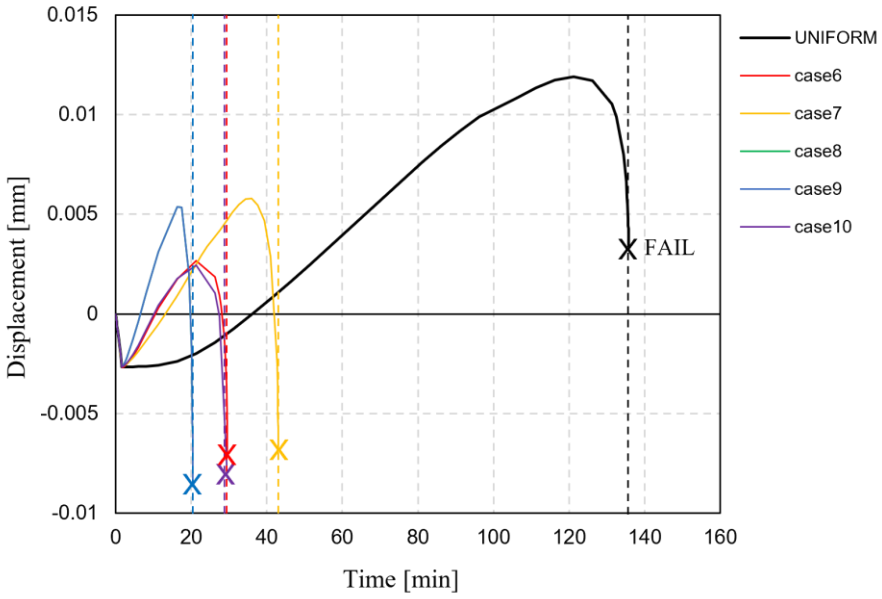

(b) Thermal gradient along the web (H-S)

Figure 5.3 Change in displacement over time

Table 5.2 presents the average temperature at fail and failure time for each case. In the case of weak axis (H-W), although the average temperature at fail for each case is similar to about 400℃, the failure points differ significantly. Likewise, in the case of the strong axis (H-S), the average temperature at failure is similar at around 300℃, but failure occurs at different times. Therefore, the eccentricity subjected to thermal gradients affects the failure time of the column.

Table 5.2 Failure time and average temperature at fail

	Thermal gradient along the flange (H-W)					Thermal gradient along the web (H-S)				
	Case1	Case2	Case3	Case4	Case5	Case6	Case7	Case8	Case9	Case10
Time[min]	84	52	24	24	169	30	43	20	20	29
T_{avg}[℃]	442	388	412	415	416	301	349	318	318	282

AISC 360-22 maintains the position that non-uniform heating can be disregarded and advocates for using uniform heating in design. This means that it suggests that a safe design can be achieved by assuming a uniform gradient with maximum temperature of the thermal gradient, as shown in Figure 5.4.

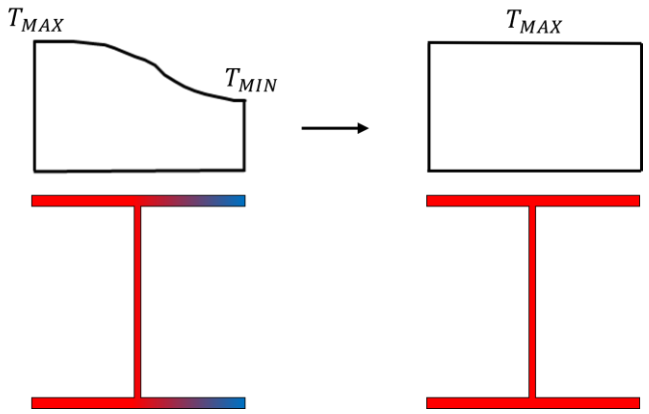

(a) column with thermal gradient (b) column with uniform gradient

Figure 5.4 Design method with thermal gradient proposed by AISC

To evaluate the design method proposed by AISC 360-22, a load heat analysis was conducted, and additional finite element analysis was performed for uniform heating. The relationship between column strength and failure temperature was obtained from the load heat analysis results, as shown in Figure 5.5. In case of the thermal gradient, the highest temperature from the gradient was applied to the graph. As a result, it can be confirmed that the strength is excessively underestimated when assume that the maximum temperature of the thermal gradient is uniformly distributed. In design, 17 to 67% of the strength subjected to thermal gradient is evaluated as the strength of uniform heating. In the worst case, designing with only 17% of the strength considering the thermal gradient leads to an extremely uneconomical design. Consequently, it is crucial to consider the effect of the thermal gradient in design.

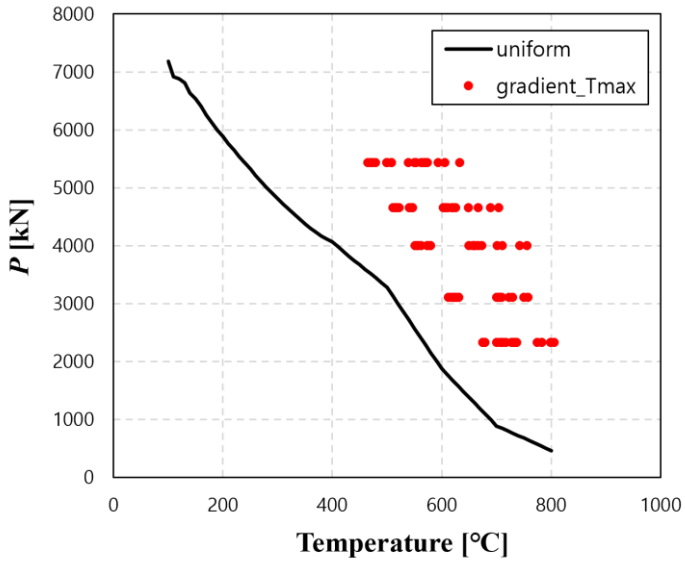

Figure 5.5 Strength of the column subjected to uniform and thermal gradient at T_{max}

5.3 Proposed design equation

The thermal gradient resulting from non-uniform heating induces eccentricity in the column. As mentioned previously, this eccentricity occurs in columns with non-uniform cross-sections and deformed columns. Due to this deformation, an additional moment is applied to the column by the original axial force, so the strength of the column must be re-evaluated considering this moment. This study proposes a *P-M* interaction curve that considers the moment caused by eccentricity, facilitating an economical design by accounting for eccentricity in the design.

The proposed equation for the *P-M* interaction is given by Eq. (5.1). It combines the axial strength of steel columns subjected to thermal gradient across the cross-section, P_{grad}, and the moment due to eccentricity, $P_{\text{grad}} \cdot e$. where, the eccentricity, e, refers to the total eccentricity obtained earlier and can be calculated using Eq. (1.1) with the eccentricity due to the shift of the stiffness center (e_{c}), thermal bowing (e_{b}), and initial imperfection (e_{i}).

$$\frac{P_{\text{grad}}}{P_{\text{cr,eff}}} + \frac{P_{\text{grad}} \cdot e}{M_{\text{p,eff}}} = 1 \tag{5.1}$$

$P_{\text{cr,eff}}$, as defined in Eq. (5.2), represents the critical buckling load at elevated temperature by modifying the nominal strength for compression at elevated temperature from AISC 360-22. If the average temperature T_{avg} is below 100 °C, the critical buckling load at room temperature modifying the nominal strength for compression at elevated temperature is applied. The reason is the

steel properties below 100 °C are the same as at room temperature.

$$P_{\text{cr,eff}} = \begin{cases} 0.658^{\left(\frac{P_{\text{y,eff}}}{P_{\text{e,eff}}}\right)} P_{\text{y,eff}} & (T_{\text{avg}} \le 100°\text{C}) \\ 0.42^{\sqrt{\frac{P_{\text{y,eff}}}{P_{\text{e,eff}}}}} P_{\text{y,eff}} & (T_{\text{avg}} > 100°\text{C}) \end{cases} \tag{5.2}$$

$P_{\text{y,eff}}$, as given in Eq. (5.3), denotes the compressive strength with the yield stress at elevated temperature, $f_{\text{y}}(T)$. The $f_{\text{y}}(T)$ can be calculated using the reduction factor for effective yield strength, k_{y} , specified in EN3.

$$P_{\text{y,eff}} = \iint_A f_{\text{y}}(T)\,\text{d}A \tag{5.3}$$

$P_{\text{e,eff}}$, according to Eq. (5.4), represents the elastic buckling load with an effective cross-section. $E(T)$ is elevated-temperature elastic modulus.

$$P_{\text{e,eff}} = \frac{\pi^2}{L^2} \iint_A E(T) \cdot \left(x - e_{\text{c}}\right)^2 \text{d}A \tag{5.4}$$

$M_{\text{p,eff}}$, as described in Eq. (5.5), corresponds to the plastic moment with the yield stress at elevated temperature, $f_{\text{y}}(T)$. Where, is distance from geometric centroidal axis and x_{PNA} is distance between centroid and plastic neutral axis.

$$M_{\text{p,eff}} = \iint_A f_{\text{y}}(T) \cdot \left|x - x_{\text{PNA}}\right| \text{d}A \tag{5.5}$$

Figure 5.6 presents the results obtained by substituting the values using the strength and temperature distribution at fail, obtained from the load heat

analysis, into Eq. (5.1). The results are classified based on column length. In the case of short columns, the dominant eccentricity is caused by the shift of the stiffness center, while in long columns, the dominant eccentricity is due to thermal bowing. When the strength obtained from load heat analysis is evaluated as a linear of *P-M* interaction curve using Eq. (5.1), it is possible to predict the strength of columns at the elevated-temperature with a moderate safety margin.

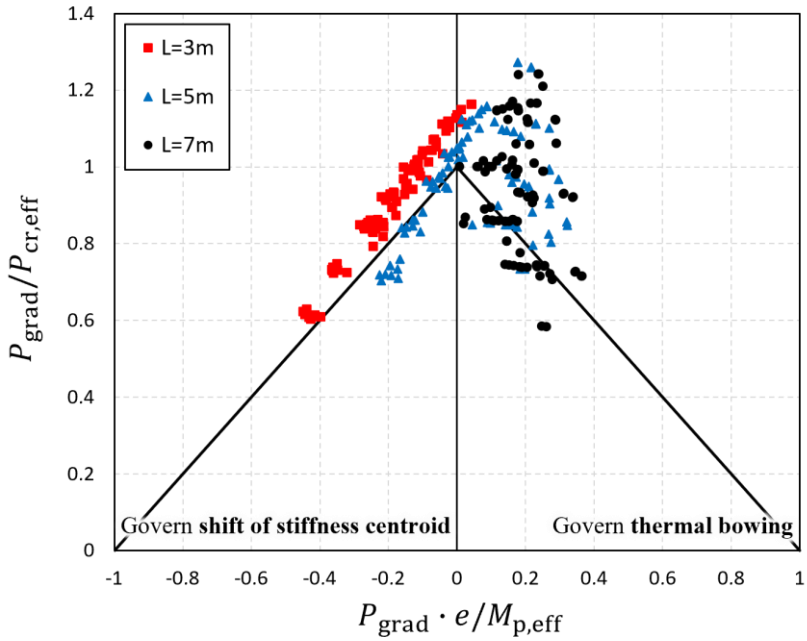

Figure 5.6 *P-M* interaction curve

Figure 5.7 and Figure 5.8 show the results of applying the FE analysis of this study to the *P-M* interaction curve considering the eccentricity from the two previous studies mentioned in Section 2.2.4. In Ojeda's study, there were values such as $\chi_{\theta_{av}}$ and κ that should be additionally obtained besides the $M_{p,\theta_{av}}$

and $P_{y,\theta_{av}}$ for the *P-M* interaction. Furthermore, the calculations of $\chi_{\theta_{av}}$, κ were not straightforward. the strength change according to the amount of eccentricity occurs without any trend. It predicts the strength of columns at the elevated-temperature as unsafe or with too much safety margin.

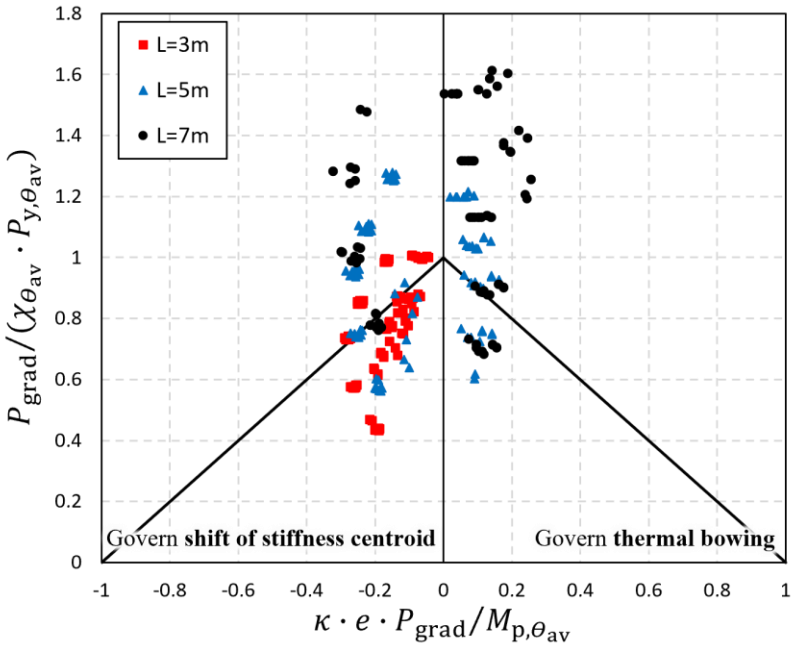

Figure 5.7 *P-M* interaction curve from Ojeda et al. (2016)

In Agarwal's study (Figure 5.8), the calculations for $P_{cr,eff}$ and $M_{n,eff}$ based on AISC 360 (2022) for *P-M* interaction are very complicated to calculate with various conditions. While the effect of eccentricity on column strength is well reflected, the study mostly predicts the strength of columns at elevated temperatures as unsafe.

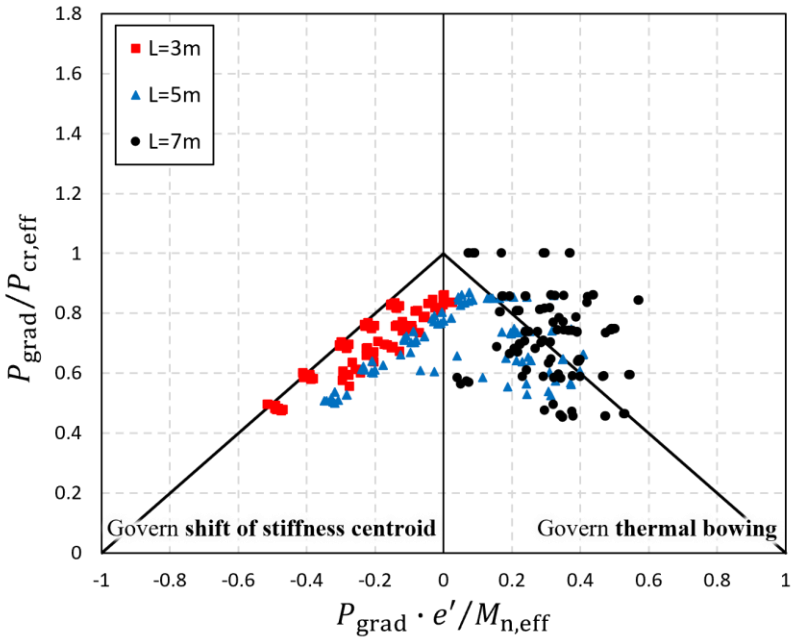

Figure 5.8 *P-M* interaction curve from Agarwal et al. (2014)

Compared other studies with this study, our study predicts the strength of columns at the elevated temperature with a moderate safety margin. Moreover, our study's normalization is simpler in calculation than other studies. In case of Ojeda and Agarwal, mean squared error(MSE) is 12.8% and 4.4% respectively. In case of our study, MSE is 4.5%. Agarwal's MSE is the lowest, but it is similar to our research, and there are many cases where it predicts as unsafe.

Chapter 6. Design Application and Example

In this chapter, we present a design procedure, design flow chart, and a solved example for applying the simple equation to calculate eccentricity and P-M interaction considering the moment due to eccentricity as presented in our research. By following the procedure outlined in this study, it is possible to achieve a reasonable fire resistance design that takes eccentricity into account, such as performance-based design. In cases where specific thermal gradient data is not available, a conservative design approach is also recommended. Therefore, it is expected that the proposed design application in this study will be actively used in practical applications.

6.1 Design procedure for steel columns with fire-induced eccentricity

The specific design process is outlined below. The notation and details of the equations are specified in depth in the previous chapter.

1. The axial strength of steel columns subjected to thermal gradient across the cross-section, denoted by P_{grad}, can be estimated as follows:

$$\frac{P_{\text{grad}}}{P_{\text{cr,eff}}} + \frac{P_{\text{grad}} \cdot e}{M_{\text{p,eff}}} = 1 \tag{6.1}$$

where, e fire-induced eccentricity,

$P_{\mathrm{cr,eff}}$ effective axial strength,

$M_{\mathrm{p,eff}}$ effective plastic moment.

2. The thermal bowing effect and the shift of stiffness center should be considered into the fire-induced eccentricity e as following:

$$e = \max(e_{\mathrm{c}} - e_{\mathrm{b}} + e_{\mathrm{i}},\quad e_{\mathrm{b}} - e_{\mathrm{c}} + e_{\mathrm{i}}) \tag{6.2}$$

where, e_{c} eccentricity due to shift of stiffness center,

e_{b} eccentricity due to thermal bowing,

e_{i} initial imperfection, recommended to use 1/1000 of the column length.

3. The values of e_{c} and e_{b} can be calculated by one of following methods.

(1) If the temperature distribution over the cross-section is given from heat transfer analysis:

$$e_{\mathrm{c}} = \frac{\iint_A E(T)\cdot x\,\mathrm{d}A}{\iint_A E(T)\,\mathrm{d}A} \tag{6.3}$$

$$e_{\mathrm{b}} = \frac{L^2}{8}\frac{\iint_A E(T)\cdot\varepsilon_{\mathrm{T}}(T)\cdot\left(x-e_{\mathrm{c}}\right)\mathrm{d}A}{\iint_A E(T)\cdot\left(x-e_{\mathrm{c}}\right)^2\,\mathrm{d}A} \tag{6.4}$$

where, x distance from geometric centroidal axis,

T temperature at a point in the cross-section,

$E(T)$ elevated-temperature elastic modulus,

$\varepsilon(T)$ thermal elongation.

(2) If heat transfer analysis is not available:

$$e_{\mathrm{c}} = \left(a_{section} \cdot \frac{1-r}{1+r} + b_{section} d_{temp} \cdot \frac{1-\sqrt{r}}{1+\sqrt{r}} \right) \cdot \frac{h}{2} \tag{6.5}$$

$$e_{\mathrm{b}} = \left(1 + c_{section} f_{temp}\right) \cdot \left[\varepsilon_{\mathrm{T}}(T_{\mathrm{H}}) - \varepsilon_{\mathrm{T}}(T_{\mathrm{L}})\right] \cdot \frac{L^2}{8h} \tag{6.6}$$

where, a, b, d, c, and f are coefficients given in Table 4.2-4.4,

h height of the cross-section,

T_{H} maximum temperature of the cross-section,

T_{L} minimum temperature of the cross-section,

r $E(T_{\mathrm{H}})/E(T_{\mathrm{L}})$

4. The effective axial strength $P_{\mathrm{cr,eff}}$ are defined as following.

$$P_{\mathrm{cr,eff}} = \begin{cases} 0.658^{\left(\frac{P_{\mathrm{y,eff}}}{P_{\mathrm{e,eff}}}\right)} P_{\mathrm{y,eff}} & (T_{\mathrm{avg}} \le 100^{\circ}\mathrm{C}) \\ 0.42^{\sqrt{\frac{P_{\mathrm{y,eff}}}{P_{\mathrm{e,eff}}}}} P_{\mathrm{y,eff}} & (T_{\mathrm{avg}} > 100^{\circ}\mathrm{C}) \end{cases} \tag{6.7}$$

where, T_{avg} average temperature of the cross section,

$P_{\mathrm{y,eff}}$ effective plastic strength,

$P_{\mathrm{e,eff}}$ effective critical load.

5. The values of $P_{y,eff}$, $P_{e,eff}$, and $M_{p,eff}$ can be calculated as following.

$$P_{y,eff} = \iint_A f_y(T)\,dA \tag{6.8}$$

$$P_{e,eff} = \frac{\pi^2}{L^2}\iint_A E(T)\cdot(x-e_c)^2\,dA \tag{6.9}$$

$$M_{p,eff} = \iint_A f_y(T)\cdot|x-x_{PNA}|\,dA \tag{6.10}$$

where, $f_y(T)$ elevated-temperature yield stress,

x_{PNA} distance between centroid and plastic neutral axis.

6. As a conservative approximation, the thermal gradient pattern can be assumed to be "STEP" distribution.

$$T_{STEP}(x) = \begin{cases} T_H & (x \le x_{STEP}) \\ T_L & (x > x_{STEP}) \end{cases} \tag{6.11}$$

where, x_{STEP} is distance of a point from geometric centroidal axis, such that the center of stiffness is located at this point. That is, $e_c = x_{STEP}$.

7. The maximum and minimum temperatures of the cross-section can be assumed to satisfy T_H =649°C and T_{avg} =538°C, which are limit temperatures provided by ASTM E119.

6.2 Design flow chart

A design flow chart is proposed based on the design procedure mentioned above. It provides an overview of the overall design process. As a result, it shows that the design using the proposed simple equation and *P-M* interaction with eccentricity is possible. (Continue on the next page)

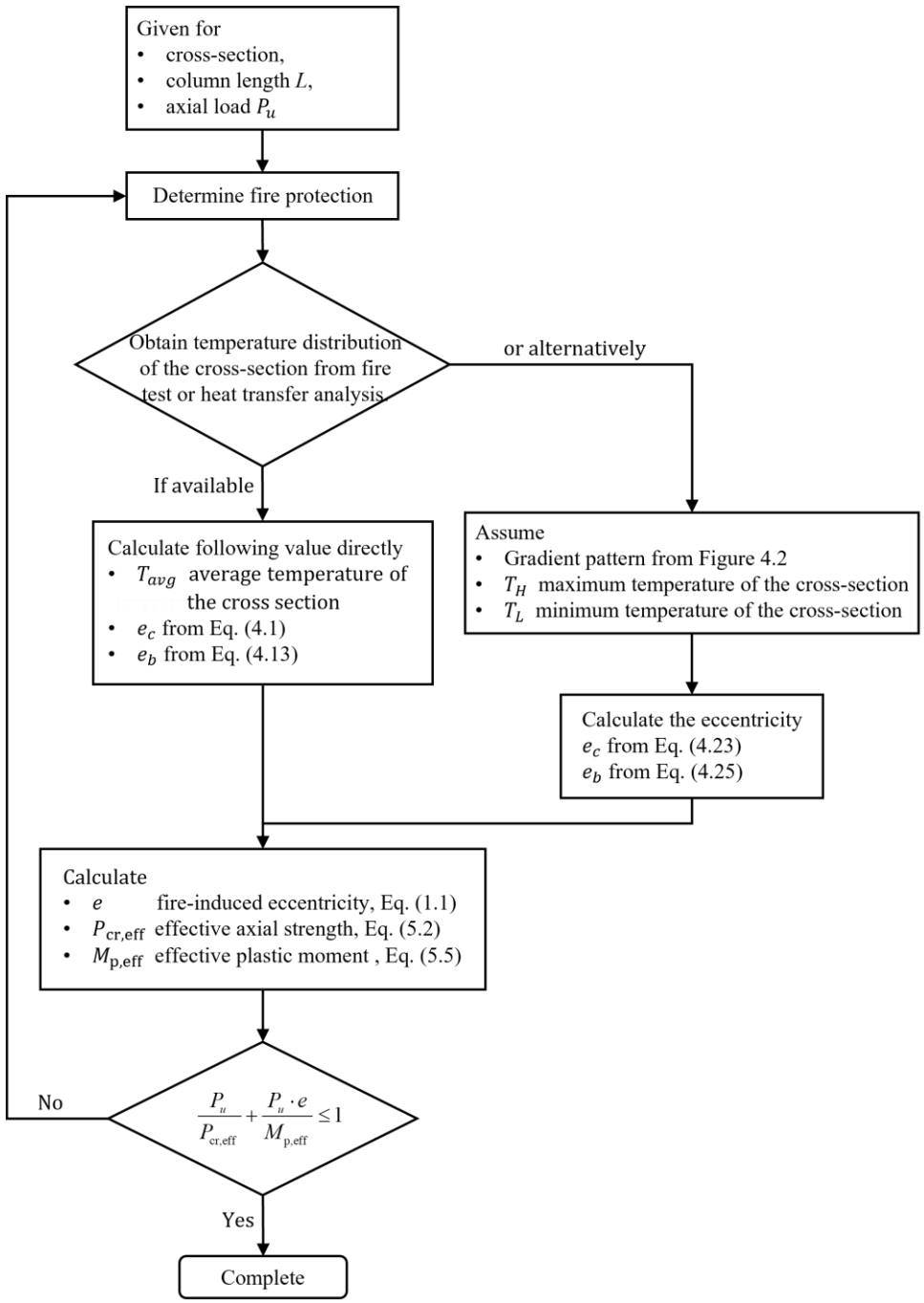
Given for
• cross-section,
• column length L,
• axial load P_u
Determine fire protection
Obtain temperature distribution of the cross-section from fire test or heat transfer analysis
or alternatively
If available
Calculate following value directly
• T_{avg} average temperature of the cross section
• e_c from Eq. (4.1)
• e_b from Eq. (4.13)
Assume
• Gradient pattern from Figure 4.2
• T_H maximum temperature of the cross-section
• T_L minimum temperature of the cross-section
Calculate the eccentricity
e_c from Eq. (4.23)
e_b from Eq. (4.25)
Calculate
• e fire-induced eccentricity, Eq. (1.1)
• $P_{cr,eff}$ effective axial strength, Eq. (5.2)
• $M_{p,eff}$ effective plastic moment , Eq. (5.5)
No
$\frac{P_u}{P_{cr,eff}} + \frac{P_u \cdot e}{M_{p,eff}} \leq 1$
Yes
Complete

6.3 Design example

This chapter presents s solved equation for a simple supported H-400x400x13x21 column with column length equal to 4m. The elastic modulus is 210,000 MPa and the yield stress is 355 MPa. To show the most conversative case, the thermal gradient along the flange (equal to H-W) is selected. We can assume that the column is exposed the standard fire from ASTM E119.

When design for fire, there are various situations. The first scenario is when the thermal gradient of the cross-section can be obtained from fire test or heat transfer analysis. The second scenario is when we can guess the approximate trend of thermal gradient and know the highest temperature of thermal gradient and the lowest temperature. the third scenario is similar with the second but there are no data of the highest and lowest temperature. The last scenario is when we can't guess any trend of thermal gradient and specific temperatures of thermal gradient. If the last scenario can be calculated, all examples can be calculated. A calculation of the last scenario is shown as below.

Scenario . when there is no data about thermal gradient :

When data for thermal gradient cannot be predicted, it is possible to conduct the most conservative fire-resistance design considering the eccentricity.

First, the stray-applied fire-resistant material (SFRM) "CAFCO 300" is selected for 2hr FRR.

Next, we have to assume the thermal gradient pattern. When the temperature gradient can't be predicted, STEP can be selected for the most conservative

thermal pattern. The specific temperature of thermal gradient can be assumed by ASTM E119. The maximum temperature is 649℃ and the minimum temperature is 427℃. Figure 6.1 shows the thermal gradient for this situation.

Now, we need to calculate the eccentricity caused by the STEP thermal gradient. The eccentricity is influenced by three factors:

1) The eccentricity due to the initial imperfection is 4mm (equivalent to $L/1000$).
2) The eccentricity resulting from the shift of stiffness center e_c can be obtained using Eq. (4.23), which consists of coefficients $a_{section}$, $b_{section}$, and d_{temp}. In this case (the weak axis of the H-beam), coefficients $a_{section}$ and $b_{section}$ applied to Eq. (4.23) are 0 and 0.9, respectively. As $a_{section}$ (equal to 0) is multiplied by the eccentricity of the flange section $(e_c)_{\substack{\text{FLN}\\0}}$, $(e_c)_{\substack{\text{FLN}\\0}}$ need not be obtained. Since the temperature gradient was previously set to STEP, a value of 1 is applied to the coefficient d_{temp} that reflects the temperature gradient. By calculating the eccentricity of RECT and STEP $(e_c)_{\substack{\text{RECT}\\\text{STEP}}}$, which are presented in Table 4.1, we can obtain the eccentricity of H-W and STEP conditions $(e_c)_{\substack{\text{H-W}\\\text{STEP}}}$. For this calculation, the material properties dependent on the temperature are used based on the values suggested by Eurocode. $(e_c)_{\substack{\text{RECT}\\\text{STEP}}}$ is calculated to be 54.12mm. Substituting the calculated values and coefficients into the simple equation, the eccentricity of the H-shaped section and STEP condition $(e_c)_{\substack{\text{H-W}\\\text{STEP}}}$ is determined to be 48.70mm.

3) The eccentricity due to thermal bowing e_b is given by Eq. (4.25). As it is an H-shaped section and its weak axis, the coefficient $c_{section}$ is 0.6. Since it is the STEP condition, the coefficient f_{temp} is 0. Additionally, the amount of eccentricity under the FLANGE and LINEAR $(e_b)_{\substack{\text{FLN}\\\text{LIN}}}$ conditions is 18.10mm, which is calculated from Eq. (4.19). Since f_{temp} is 0, $(e_b)_{\substack{\text{H-W}\\\text{STEP}}}$ is equal to $(e_b)_{\substack{\text{FLN}\\\text{LIN}}}$.

As a result of calculating the maximum eccentricity (e) occurring on the column using the previously calculated values, it is determined to be 34.60 mm.

To evaluate the strength of the column, the effective axial strength ($P_{\text{cr,eff}}$) and the effective plastic moment ($M_{\text{p,eff}}$) must be calculated. These two values are given by Eq. (5.2) and Eq. (5.5), respectively. Figure 6.1 shows the discretization of the column section and the values of temperature, yield stress, and elastic modulus. When these values are used in the calculation, the effective axial strength ($P_{\text{cr,eff}}$) is determined to be 2370.86 kN, and the effective plastic moment ($M_{\text{p,eff}}$) is calculated to be 349.39 kN.

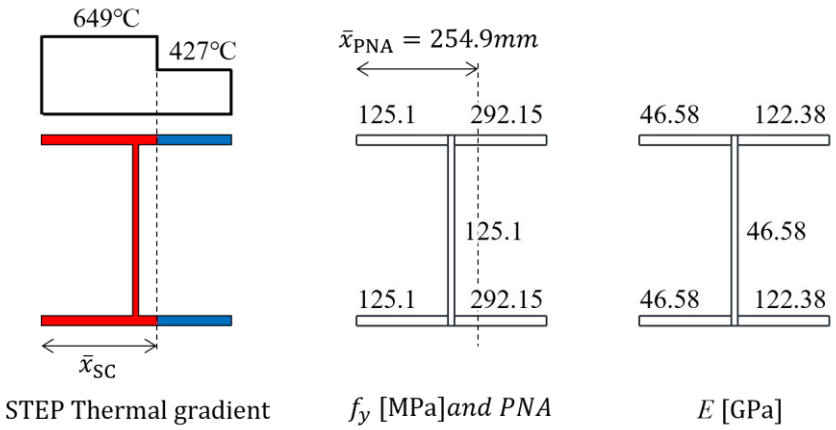

Figure 6.1 Discretization of the column section and the value of temperature, yield stress, and elastic modulus

Where, $\bar{x}_{sc}$ is the distance from the end of the column to the stiffness center.

Finally, by substituting the calculated values into Eq. (5.1), the load capacity P in a given fire situation is calculated as 1920.06 kN.

Chapter 7. Conclusion and Summary

This study focused on investigating the behavior of steel columns under fire. First, heat transfer analysis is conducted to analyze the potential temperature distributions over the cross-section of steel columns under real fire scenarios. Subsequently, based on the given highest and lowest temperatures of the thermal gradient, we proposed a simple equation to predict the eccentricity. Lastly, a new design equation is introduced, considering the eccentricity through load heating analysis. The conclusions of this study can be summarized in five points.

(1) Current design standards do not adequately account for the effects of thermal gradients, despite their significant impact on the fire resistance and strength of columns.

(2) To analyze the thermal gradients that can occur over the cross-section of a steel column, we performed heat transfer analysis using five real fire scenarios. As a result, we categorized the thermal gradients into three types: "LOW" dominated by low temperature, "LINEAR" with a linear gradient, and "HIGH" dominated by high temperature.

(3) We proposed a simple equation to calculate the eccentricity caused by various thermal gradients obtained from the heat transfer analysis. Specifically, we presented two equations to predict the eccentricity due to the shift of the stiffness center and the eccentricity due to thermal bowing, respectively. The

eccentricity of the H-shaped section can be predicted by multiplying the coefficient of each condition by the specific eccentricity that can be easily calculated using the thermal properties at the maximum and minimum temperatures.

(4) In order to investigate the effect of eccentricity induced by thermal gradients on the behavior of steel columns, load heating analysis was performed with various load and slenderness ratios applied. As a result, it was confirmed that rapid thermal gradients significantly affect the fire resistance performance of the columns.

(5) Based on the numerical analysis, a design equation considering the moment induced by eccentricity was proposed. Compared to existing design equations, the new proposed design equation predicts the strength of columns with thermal gradients as safe.

References

[1] AISC-360. (2022). *Specification for Structural Steel Buildings*. Chicago : American Institute of Steel Construction.

[2] AISC-360. (2016). *Specification for Structural Steel Buildings*. Chicago : American Institute of Steel Construction.

[3] EN 1993-1-2. (2005). *Eurocode 3: Design of Steel Structures, Part 1-2: General Rules – Structural Fire Design.* Brussels, Belgium : CEN.

[4] Agarwal A, Choe L, Varma AH. (2014). *Fire design of steel columns: effects of thermal gradients*. Journal of Constructional Steel Research, 93, 107–18.

[5] Dwaikat MMS, Kodur VKR, Quiel SE, Garlock MEM. (2012). *a simplified approach for predicting temperature profile in steel members with locally damaged fire protection*. Fire Technology, 48, 493–512.

[6] Becker R. (2002). *Structural behavior of simple steel structures with non-uniform longitudinal temperature distributions under fire conditions*. Fire Safety Journal, 37, 495–515.

[7] Yang K-C, Lee H-H, Chan O. (2009). *Experimental study of fire-resistant steel H-columns at elevated temperature*. Journal of Constructional Steel Research, 62, 544–53.

[8] Ojeda OD, Maljaars J, Abspoel R. (2016). *Fire exposed steel columns with a thermal gradient over the cross-section.* Thin-Walled Structures, 98, 103-110.

[9] Agarwal A. (2011). *Stability Behavior of Steel Building Structures in*

Fire Conditions (Doctoral dissertation). Retrieved from https://www.proquest.com/docview/1015155670?pq-origsite=gscholar&fromopenview=true.

[10] Yang K-C, Rejia H. (2009b). *Structural behavior of centrally loaded steel columns at elevated temperature*. Journal of Constructional Steel Research, 65, 2062–2068.

[11] Wang W-Y, Li G-Q, Kodur V. (2013). *Approach for Modeling Fire Insulation Damage in Steel Columns*. JOURNAL OF STRUCTURAL ENGINEERING, 139, 491-503.

[12] Tomecek DV, Milke JA. (1993). *A Study of the Effect of Partial Loss of Protection on the Fire Resistance of Steel Columns*. Fire Technology First Quarter.

[13] Isolatek International (2008) CAFCO 300 guide specifications. Stanhopehttps://www.isolatek.com/wp-content/uploads/2020/10/CAFCO-300_C-TDS_10-20.pdf

[14] Choe L. (2011). *Structural mechanics and behavior of steel members under fire loading* (Doctoral dissertation). Retrieved from https://www.proquest.com/docview/1015155669?pq-origsite=gscholar&fromopenview=true.

[15] Talamona D, Franssen JM, Schleich JB, Kruppa J. (1997). *Stability of steel columns in case of fire: numerical modeling*. JOURNAL OF STRUCTURAL ENGINEERING, 123(6), 713–20.

[16] Boon W. (2014). The Influence of thermal gradients in steel columns due to pool fires (Master's thesis). Retrieved from https://repository.tudelft.nl/islandora/object/uuid:f3f96dc7-2339-4751-9110-7edbf6f6ff2d

[17] Takagi J, Deierlein GG. (2007). Strength design criteria for steel members at elevated temperatures. Journal of Constructional Steel Research, 63,1036–50.

초 록

화재 시 단면내 온도구배 하중을 받는 강재기둥의 강도 해석

소 원

서울대학교 건축학과 대학원

건축물에 화재가 발생할 경우 화재 자체의 비균질성 뿐만 아니라, 방화구획 등으로 인한 열 유입 제한, 노후화로 인한 내화 피복재 부분 탈락 등 다양한 원인으로 인해 기둥 단면 내에 온도 구배가 발생하게 된다. 이러한 온도 구배는 불균일한 열팽창으로 인해 기둥이 휘는 열굽힘 현상과 단면의 도심과 일치하던 강성 중심이 온도 구배 형성에 따라 이동하는 현상을 유발한다. 이로 인해 기둥에 편심이 발생하여 기둥의 내화 성능 뿐만 아니라 강도를 떨어뜨릴 수 있다. 현행 설계 기준에서는 온도 구배로 인한 영향을 고려하는 구체적인 설계 방안에 대해 제시하고 있지 않다. 본 연구에서는 실제 화재 상황을 가정한 다섯가지 가열조건에 대해 열전달 해석을 수행하고 H형강 기둥 단면 내 발생하는 온도 구배 패턴을 분석하였다. 그 결과, 온도 구배 패턴을 크게 고온지배적, 직선형, 저온지배적 등 세가지 유형으로 분류할 수 있었고, 이를

초 록

바탕으로 단면 내 최고 온도와 최저온도가 주어졌을 때 편심 발생량을 예측할 수 있는 간단 계산식을 제안했다. 한편, 화재로 인한 편심이 기둥 강도에 미치는 영향을 확인하고자 다양한 하중비를 받는 기둥에 대해 재하 가열 해석을 수행했다. 그 결과, 단면 내 평균온도와 최고온도가 더 낮음에도 불구하고 급격한 온도 구배로 인해 내화 성능 시간이 더 짧을 수도 있음을 확인했다. 기둥 압축력과 온도 구배 편심에 따른 휨 모멘트 사이의 P-M 상관 관계를 제안하였으며, 기존 설계 기준에 비해 온도 구배가 있는 기둥의 강도를 보수적으로 잘 예측하였다.

주요어 : 내화구조; 온도구배; 열굽힘; 기둥 편심; 철골기둥;

학 번 : 2021-29074